Experimental and numerical analysis on serviceability of cantilevered floor based on human-structure interaction

Qiankun Zhu*[1,2a], Kaifang Liu[1b], Lulu Liu[3a], Yongfeng Du[1c], Stana Zivanovic[2b]

[1]*Institute of Earthquake Protection and Disaster Mitigation, Lanzhou University of Technology, Lanzhou, Langongping Road 287, 730050, China*

[2]*College of Engineering, Mathematics and Physical Science, University of Exeter, North Park Road, EX4 4QF Exeter, UK*

[3]*College of Civil Engineering, Southeast University, Nanjing 211189, China*

Abstract: To evaluate the vibration serviceability of structure under human-induced excitation, experimental and numerical analysis were conducted on a cantilevered floor of a gymnasium, which was assumed as a case study. A series of field tests were performed using the ambient excitation and the human excitation approaches on the floor to obtain the fundamental vibration characteristics and human-induced response, respectively. Finite element models (FEMs) of the cantilevered floor were established, modified and validated according to the field test results and the weak constraint effect of glass curtain walls was proposed in this paper. The numerical analysis of human-induced vibration was conducted by considering the pedestrian load as the combination of the Fourier series load model and the mass-spring-damper (MSD) human dynamic model. To better simulate the human-structure interaction (HSI), both the main-harmonics and sub-harmonics load spectra were considered for the equivalent load model due to the characteristics of narrow bands. The results showed that both structural vibration modes and human-induced acceleration responses were in good agreement compared with experimental results. The weak constraint effect of glass curtain walls was then validated. The numerical results were more accurate when considering the influence of HSI on the structural vibration serviceability in practical engineering applications.

Keywords: Cantilevered floor; Human-structure interaction; Field tests; FEM; Vibration serviceability; Weak constraint effect of glass curtain walls; Sub-harmonics components.

1. Introduction

With the emerging of high-strength and light-weight materials, numerous large-space structures, such as gymnasium, have been constructed in the public buildings. Large-span structures usually behave with flexibility and low natural frequency which is more close to the main-band of low-frequency dynamic loads such as pedestrian excitation. If such loads are enforced into these structures, unexpected large dynamic response even catastrophic damage might occur. Therefore, apart from the basic design requirement of ultimate limit state and serviceability limit state, more attention should be given on the potential problem of human-induced vibration in large-span structures regarding the vibration serviceability. [1–3].

Obtaining accurate structural mode shape and fundamental frequency is the prerequisite for the numerical analysis of vibration serviceability evaluation. Previous studies have indicated that the vibration characteristics of the floor were affected by the existing of non-structural components, such as decorative floors and glass curtain walls. Devin et al. [4] showed that the floor stiffness and natural frequencies was increased by 30% and vibration modes were significantly changed

*Corresponding author, Professor, E-mail: zhuqklut@qq.com

considering the non-structural components. Similar conclusions also addressed in [5–11] that the structural vibration mode was changed after installation of some non-structural components and inner walls. Fanning et al. [12] and Pavic et al. [13] experimentally and numerically evaluated the effects of the non-structural partition on the vibration of multi-story concrete buildings. It showed that the floor vibration was caused by its inherent excitation, and some insignificant vibration transmitted through structural and non-structural components due to the simultaneous activity among different stories of the floors. The glass curtain walls, as a large non-structural component with a space system consisted of glass, skeleton and row-columns provided a boundary condition for the floor. The effect of glass curtain walls on the vibration characteristics was usually equivalent as additional mass and stiffness applied on the floor [4]. However, based on this equivalent method, the numerical analysis was hard to obtain a good agreement with the experimental results. Thus, an improved equivalent approach should be developed to consider the constraint effect of glass curtain walls on the floor.

The numerical analysis of human-induced vibration in FE model can be realized by considering the pedestrian load as a Fourier series load model [14–17]. Živanović et al. [18] concluded that the sub-harmonics spectrum between the main-harmonics could not be ignored, which affected the pedestrian load based on the data analysis conducted by Brownjohn et al. [19]. Therefore; the Fourier load model was revised. Subsequently, some studies found that human occupied in the structure also had an effect on the structural vibration frequency and damping, even the vibration response, which was known as HSI in the practical structure [20–23]. Hence, the HSI should not be ignored in numerical analysis. Kim et al. [24] employed a biomechanical model to evaluate the HSI for a single pedestrian, and showed that was in good agreement with the experiment results. Based on the pedestrians' acceleration data measured in the field tests, Silva [25] proposed a single-degree-of-freedom human body dynamic model to simulate the vertical dynamic characteristics of pedestrians and structures. The mass, stiffness, and damping of the model were the function of the human body weight and walking frequency. Da et al. [26] and Dang [27] investigated the vertical dynamic HSI based on the human body dynamic model. However, the effect of pedestrians on dynamic characteristics of the structure was not discussed in depth. Thus, based on the above research, in addition to employ the Fourier series load model to represent the pedestrian load, the sub-harmonics spectrum and a single-degree-of-freedom of mass-spring-damper (MSD) system should also be developed to characterize the HSI for the numerical vibration analysis.

Currently, numerous studies have been done experimentally and numerically on the human-induced vibration and structural serviceability evaluation, such as footbridge, large-span floor [28–33]. However, a complete analysis for the human-induced vibration based on the HSI and non-structural components have not been presented. Limited research has been investigated for the vibration response of cantilevered floors whose maximum deformation and response occurs often in the end of cantilever structures distinguished from the ordinary floor. Thus, a comprehensive study is necessary to experimentally and numerically investigate the effects of human-induced vibration on the floor considering the HSI and the non-structural effect.

The outline of this paper is as follows: a brief description of the gymnasium building was given in Section2, including the characteristics of structural elements and floors. The experimental mode of the floor was presented from field tests and the FEM based on the proposed weak constraint effect of glass curtain walls was updated in Section3. The acceleration field test on the

floor under pedestrians' excitation was conducted in Section 4, and the sub-harmonics in the force spectrum were explained. Then, a comparison of the acceleration response obtained from FEM results and field tests were presented and the effect of HSI on the vibration serviceability of structures was highlighted. Finally, the main discussion and conclusions were summarized in Sections 5 and 6, respectively.

2. Structural basic information

The gymnasium is located in the Northwest of China, with a total construction area of 51800 m^2. This building consists of two main parts: main truss structural system and suspension structure which cantilevers overhanging the former one, mainly serving as competition and training place for athletes. The investigated cantilevered floor is a part structure of the gymnasium, overhanging 15.0 m at an elevation of 13.5 m, as shown in Fig. 1. Its main function is the lounge and exhibition as a gathering place for personnel.

(a) (b)

Fig. 1. Front view (a) and left view (b) of the cantilevered floor structure under construction.

The cantilevered part consists of a steel frame-support structure where the load is transfer by the cantilever beam into the column. Two type of beam sections are selected, i.e., box-type and H-type. The top steel beam is also supported by a diagonal brace to strengthen the structural stiffness, as shown in Fig.1. Two layers of the floors between trusses are connected by pillars and slings at the cantilevered end, which are the main load-bearing elements in the cantilevered end. The steel truss deck as a new structural type is used in the floor system, with a thickness of 180 mm. In order to satisfy the requirements of architectural design for the permeability of sunlight, a large-span glass curtain wall is installed along the cantilevered end. The cross-section of the whole gymnasium and plan of the cantilevered truss are shown in Fig. 2. The main structural components supported the floor are listed in Table 1.

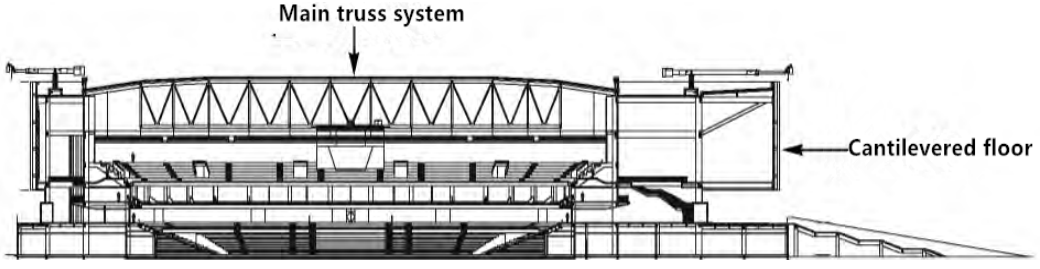

(a)

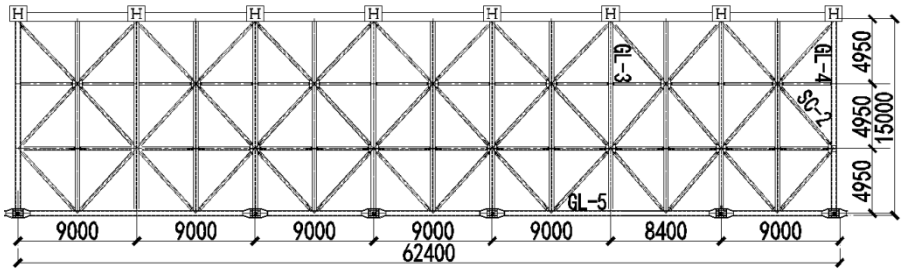

(b)

Fig. 2. Cross-section (a) and plan (b) of the building.

Table 1

Parameters of structural components supported the cantilevered floor

Component items	Sectional specification	Section type	Remarks
GL3	H1000×350×20×24	Welding H shape	secondary-beam
GL4	B1000×400×20×24	Welding rectangle	secondary-beam
GL5	B1000×400×20×24	Welding rectangle	main-beam
SC2	P 245×8.0	Hot rolling seamless	Horizontal support

3. Modal analysis for the cantilevered floor

3.1 Field test preparation

The ambient excitation test was conducted on the cantilevered floor to obtain the dynamic properties of the gymnasium and validate the FEM. The modal testing was conducted when the major structure was completed but has not opened to the public. As the floor vibration test is greatly influenced by the external environment, the test time is selected at night to eliminate its interference and obtain the ideal natural pulsation signal. The general arrangement of the field test is shown in Fig. 3, and the modal tests were performed using a 941B accelerometer and INV3060V acquisition system.

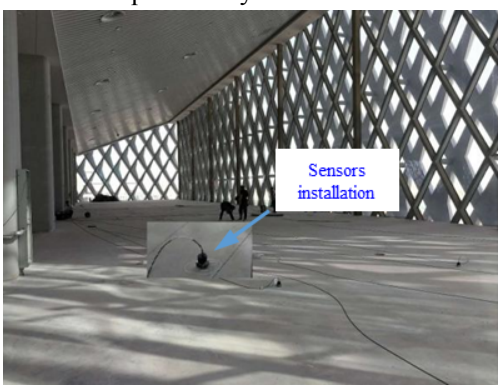

(a)

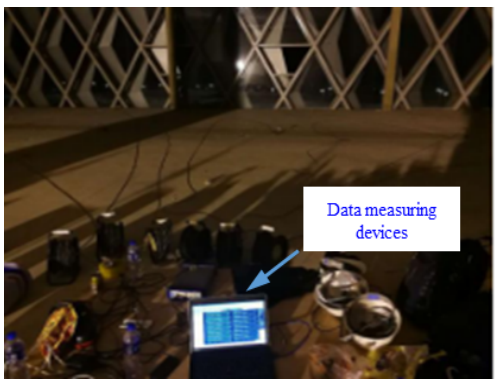

(b)

Fig. 3. Field test: (a) installation of the accelerometers (b) data measuring devices.

85 test points in total were selected in this test for placing accelerometers to accurately map mode shapes. As the existing equipment cannot complete the data collection for all measuring points at one time, alternatively using the accelerometers in the test points was performed for multiple times. For example, #1, #6, #11, #16, #21, #26, #31 and #36 were the first group of the test points; after the data were collected, the accelerometers were moved to the next group points based on the specified order along the beam row after row, as shown in Fig. 4. As a result, ten groups were needed for the whole data acquisition. In order to identify multiple sets of data

together, the #76 point was selected as the reference point and recorded every test; the sampling frequency was 256 Hz, and correspondingly, the record times were 15 minutes for each setup.

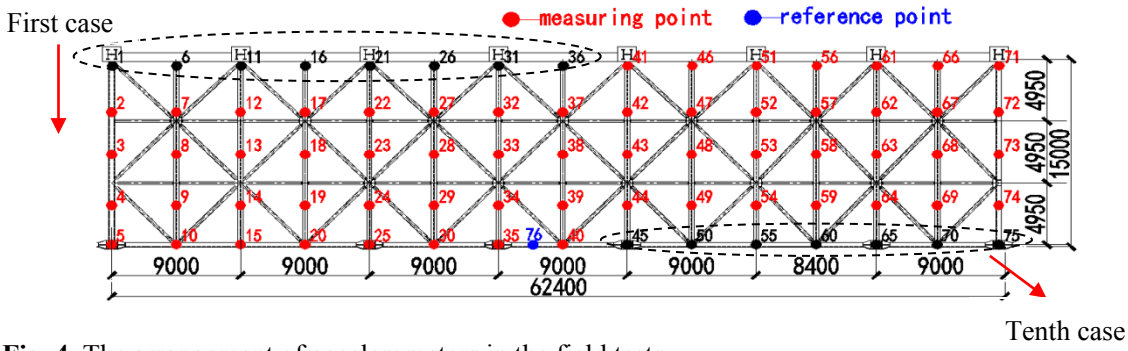

Fig. 4. The arrangement of accelerometers in the field tests.

3.2 Field test results for mode shapes

The stochastic subspace identification (SSI) approach was used to process the data. The frequencies of six vibration modes were obtained directly as follows: 3.36, 4.13, 5.23, 6.63, 7.38, and 8.08 Hz. The experimental vibration modes are shown in Fig. 5. It could be concluded that the fundamental frequency of the structure meets the requirement of the code of AISC Design Guide 11 (Murray et al. 2016) [34]: The frequency of the large-span public buildings should not be less than 3 Hz. As the first vertical frequency was still rather low, the vibration serviceability evaluation was conducted in the following parts.

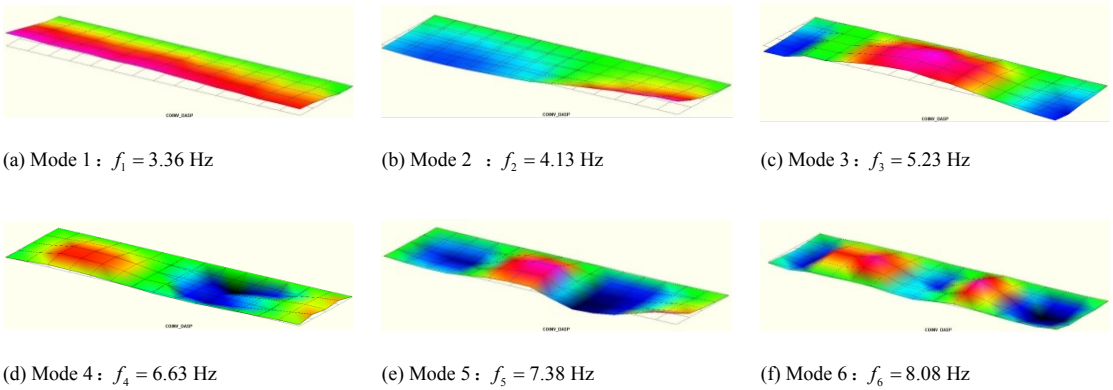

(a) Mode 1：$f_1 = 3.36$ Hz (b) Mode 2 ：$f_2 = 4.13$ Hz (c) Mode 3：$f_3 = 5.23$ Hz

(d) Mode 4：$f_4 = 6.63$ Hz (e) Mode 5：$f_5 = 7.38$ Hz (f) Mode 6：$f_6 = 8.08$ Hz

Fig. 5. Natural frequencies and mode shapes determined by the SSI approach.

3.3 Numerical analysis for mode shapes

3.3.1 FEM of the cantilevered floor

APDL language was used in ANSYS to define material properties, input component parameters, select the element type, establish the model, and obtain the results. In this study, BEAM188 element (a kind of 3D linear elements) was used to simulate the steel truss, the cantilevered column, and the steel beam at the bottom of the slab, whose Young's modulus, density, and PRXY is $2e^{11}$ N/mm, 7850 kg/m^3 and 0.3, respectively; SHELL181 element was selected to model the concrete slab, whose Young's modulus, density, and PRXY is $3.15e^{10}$ N/mm, 2550 kg/m^3, and 0.2, respectively; while LINK180 element was employed to simulate the slings, web bars, and struts. Due to the complexity of the glass curtain wall system, MASS21 element was chosen to simplify the simulation of the glass curtain wall. In the FEM, each component was created by its own node; different components might have coincident nodes at the connection parts;

the connection between different components of the overall structure was achieved by merging nodes at the same location; after merging, only one node was formed in the same location, as shown in Figs. 6 (a) – (b).

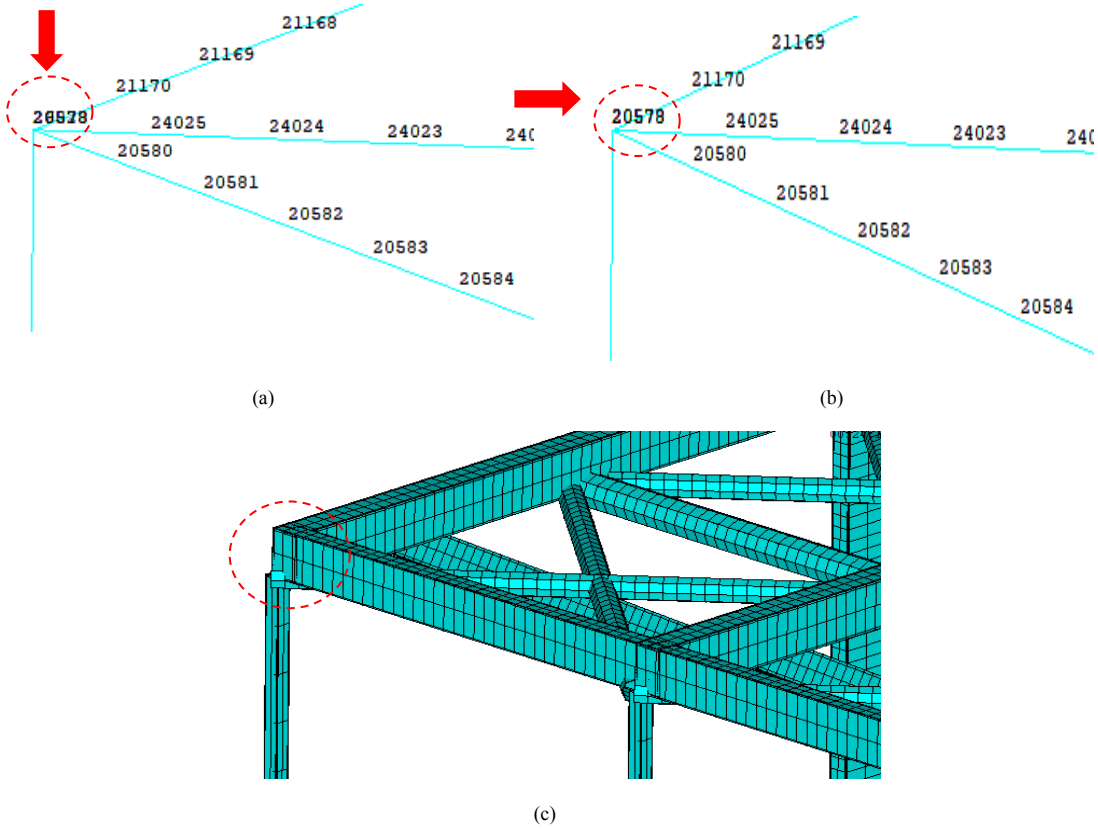

(a) (b)

(c)

Fig. 6. Merging different components: (a) before merging (b) after merging (c) connection between different components.

The established model of the cantilevered structure is shown in Fig. 7 (a). An accurate definition of the boundary conditions is also the key to obtain the true dynamic response analysis. In the practical structure, the constraint between beams and columns is a semi-rigid constraint between hinge and fixed condition. Spring elements were used to simulate this constraint state in FEM. Considering the vibration modal of the cantilevered floor, the constraint condition was defined as below, the translational freedoms UXYZ except UZ and the rotational freedom were fixed, releasing the axial constraint UZ between beams and columns; the axial spring damper COMBIN14 was used to further simulate the slip between beams and columns as shown in Figs. 7 (b) – (c).

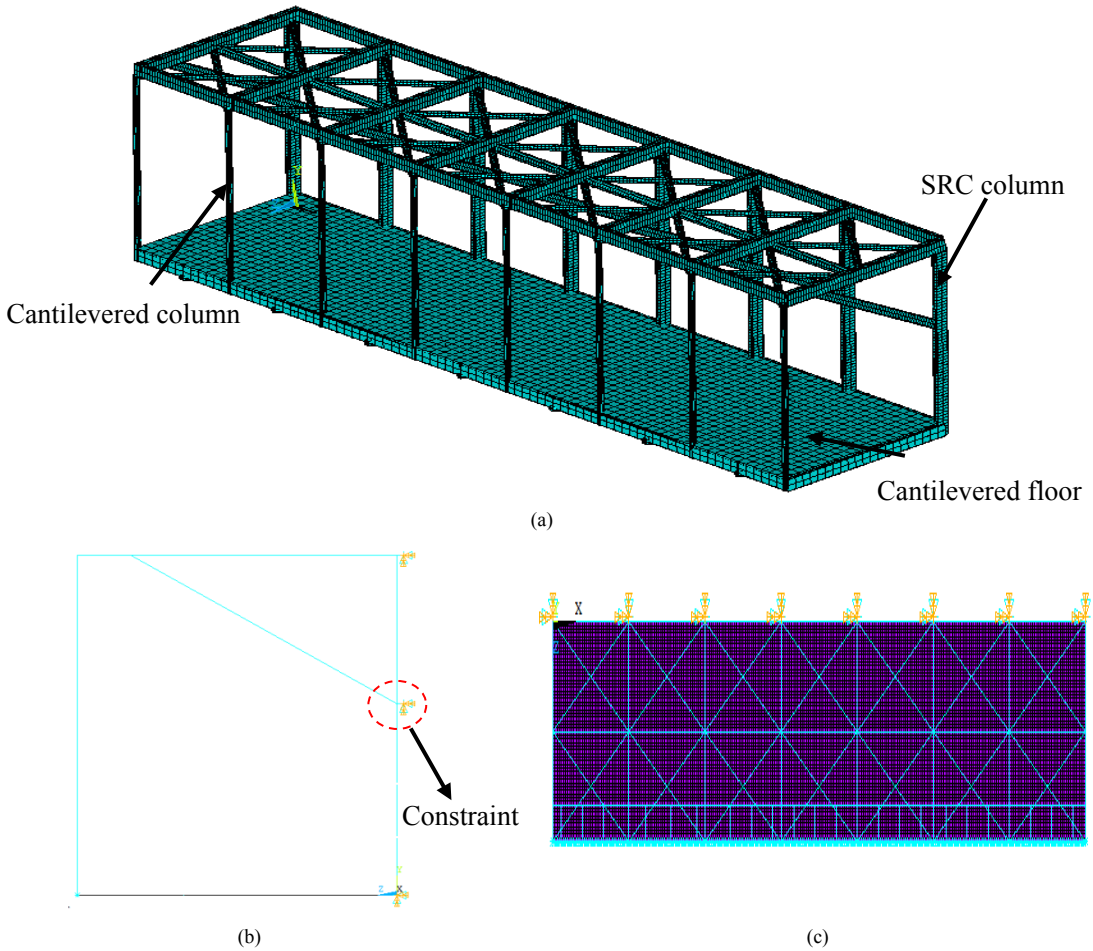

Fig. 7. FEM: (a) element shape of isometric view (b) right view (c) top view

3.3.2 Equivalent approaches for glass curtain walls in numerical analysis

The analysis of the effect of glass curtain walls on structural behavior was always simplified in the current study to consider the interaction between glass curtain walls and the integral structure. Two widely used approaches exist: the one is that glass curtain walls are simplified as equivalent mass distributing along its position (approach I); the other is as the equivalent vertical stiffness contributing to the structure (approach Π) [4].

These two approaches were applied firstly to evaluate the effect of the glass curtain walls on the structural dynamic behavior and the results are shown in Table 2. Comparing the modal results between field tests and FEM analysis, adopting the existing equivalent approaches for the glass curtain walls cannot agree well with the experiment results. The mode1 frequency of the floor using the equivalent approach I for the glass curtain wall was 2.80 Hz, and the error was 16.67% compared with the experimental value of 3.36 Hz. While for the approach Π, the value was 2.82 Hz with an error of 16.07%. Moreover, the following frequencies were also underestimated with large difference and the mode shapes differed greatly compared with the experiment. The deviation occurred in the approach I could be explained: the contribution of glass curtain walls to floor stiffness was neglected even though the weight of glass curtain walls was considered in the current practice. For the approach II, both the contributions of glass curtain wall weight and stiffness were considered; however, only the vertical stiffness was equivalent by the axial vertical spring, neglecting the weak constraint effect of glass curtain walls. Based on the modal results, a weak constraint of glass curtain effect was proposed and further validated in FEM.

Table 2

Comparisons of the structural frequencies between the experimental and numerical results based on the two simplified approaches to the glass curtain wall

Mode	approach I (Hz)	approach Π (Hz)	Experiment (Hz)	Error between approach I and experimental (%)	Error between approach Π and experimental (%)
1	2.80	2.82	3.36	16.67	16.07
2	3.02	3.04	4.13	26.88	26.39
3	3.54	3.57	5.23	32.31	31.74
4	4.29	4.34	6.63	35.29	34.54
5	5.38	5.46	7.38	27.10	26.02
6	6.63	6.75	8.08	17.95	16.46

3.4 Updated FEM based on the weak constraint effect

To ensure the accuracy of numerical analysis, the model was updated according to the experimental results. Zhu et al. [35] proposed that the adjustability of floor frequency and different degrees of vibration reduction can be achieved by defining semi-rigid supports with different stiffness ratios. Here, the spring damper, COMBIN14, was used to simulate the slip between beams and columns. Secondly, according to the weak constraint effect of glass curtain walls, the equivalent stiffness approach was employed to study the effect of glass curtain walls on the stiffness of truss columns and then the glass curtain walls was considered in the modal calculation of floor vibration.

3.4.1 Weak constraint effect

A space system was constituted by the glass curtain walls, its skeleton and supported row-column, as shown in Fig. 8 (a). Compared with the original single row-column, the system owns a constraint effect: the in-plane lateral stiffness of the system increases by multiples of geometric series. Diamond or rectangular skeletons are generally adopted in the glass curtain walls, and the out-of-plane lateral stiffness of the wall also increases with skeleton constraints through connectors. Moreover, glass curtain walls are generally connected with row-columns through the skeleton, as shown in Fig. 8 (b); the constraint of the floor is also reinforced through row-columns, which is different from the commonly constructed wall. Because of weak linkages between elements, the lateral stiffness of the system is smaller than that of the bare wall of the same shape. The effect of the glass curtain wall on the floor structure above can be called as the weak constraint effect.

(a)

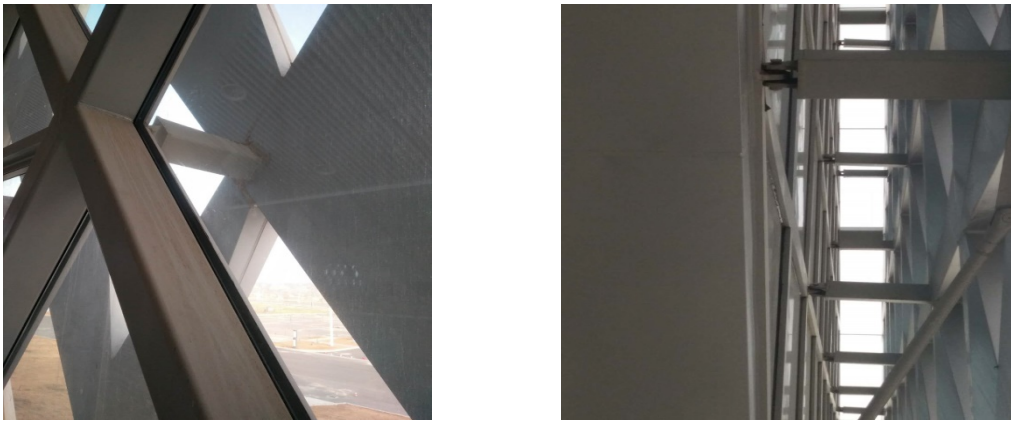

(b)

Fig. 8. On-site glass curtain wall: (a) elevation of glass curtain walls (b) connections between glass curtain wall skeletons.

The whole stiffness of the cantilevered column significantly increases due to the existing of the glass curtain walls. For example, the lattice column's stiffness is much larger than that of several single columns. Therefore, the whole inertia moment of the cantilevered column was significantly improved by the weak constraint effect. Thus, an equivalent approach was adopted to consider the role of glass curtain walls in the FEM. The equivalent mass was simulated by the MASS21 element, and the contribution of glass curtain walls to the stiffness of the floor was achieved by increasing the stiffness of the cantilevered column with equal strength. The equivalent principle in ANSYS was to increase the elastic modulus of the cantilevered column by multiple different series to achieve the weak constraint effect of glass curtain walls. The specific value was determined by the comparison with experimental results.

3.4.2 Mode comparison between the updated FEM and field tests

Referring to the experimental results of structural vibration frequencies and modes, the stiffness of the cantilevered column was increased by multiple series based on the weak constraint effect. In order to rapidly evaluate the equivalent cantilevered column stiffness of the weak constraint effect, it was assumed that the glass curtain wall and cantilevered columns were of the same material. Therefore, the ratio of out-of-plane stiffness was equivalent to the ratio of section inertia moment, in this case, the number of cantilevered columns was 8, and the section was 300 mm × 300 mm, the thickness of glass curtain wall was 200 mm, and the distance between the glass curtain wall and cantilevered column was 400 mm. The stiffness of the cantilevered column calculated with the knowledge of material mechanics was approximately 700 series of the real wall equivalent. In the real case, the moment of inertia of the equivalent cantilevered column was approximately 1:2 of the solid wall, about 350 series to 700 of the solid wall. Consequently, when the stiffness of the cantilevered column was increased by 500 series, the numerical results of vibration modes agreed well with the experimental results, as shown in Fig. 9. Here, the modal characteristics of the floor and cantilevered columns were extracted from the whole structure.

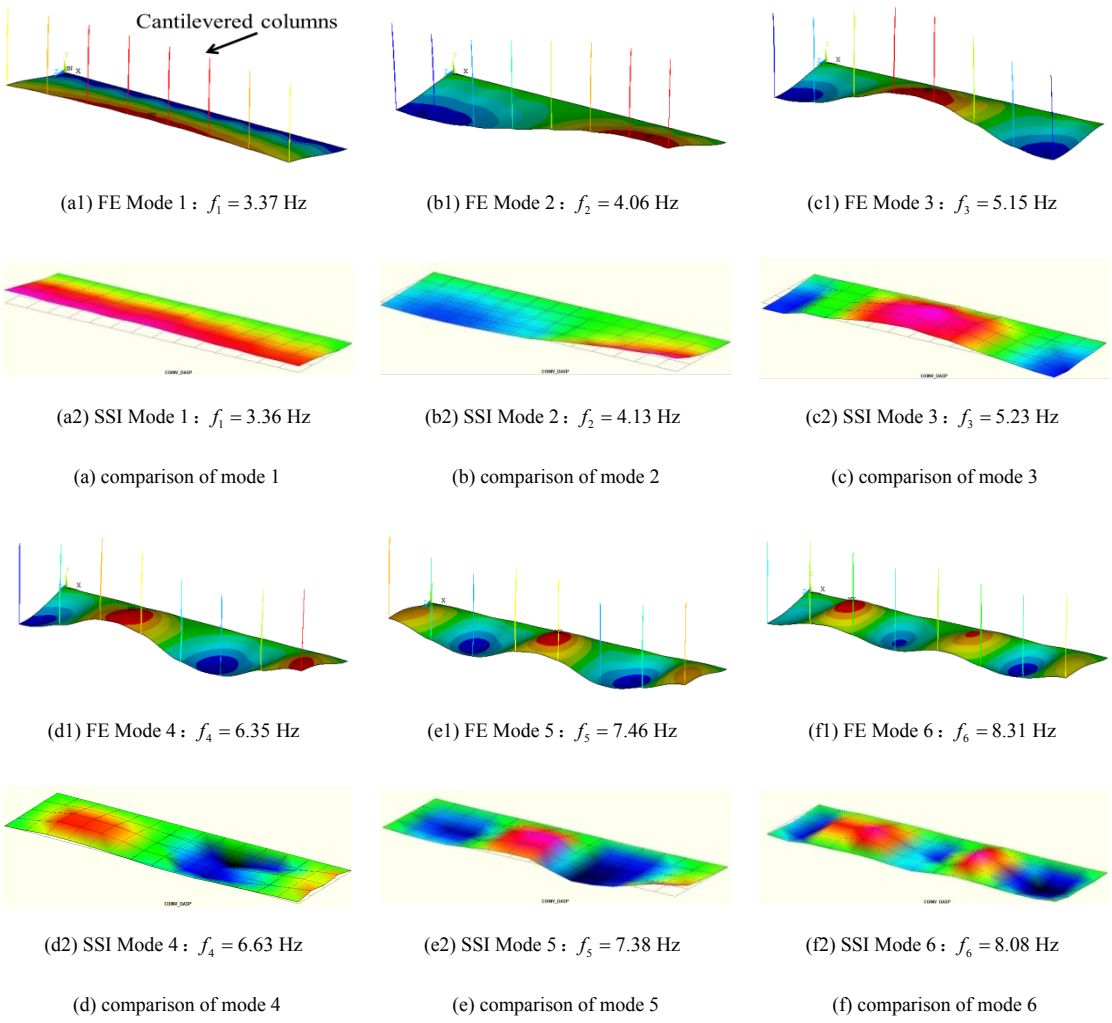

Fig. 9. Comparisons of experimental and numerical (updated model) mode shapes.

The vertical vibration frequencies obtained from the updated FEM were 3.37, 4.06, 5.15, 6.35, 7.46, and 8.31 Hz, respectively (see Table 3). The results showed that the vibration frequency between numerical and experimental results agreed well. The error of each frequency was less than 5% and average errors were 1.93%, which was an excellent satisfied result after considering the weak constraint effect. Therefore, increasing the stiffness of the cantilevered column was a reasonable way to represent the weak constraint effect.

Table 3

Comparisons of natural frequencies between experimental and numerical (updated model) results

Mode	Numerical (Hz)	Experimental (Hz)	Relative error (%)
1	3.37	3.36	0.30
2	4.06	4.13	1.69
3	5.15	5.23	1.53
4	6.35	6.63	4.22
5	7.46	7.38	1.07
6	8.31	8.08	2.77
Average error/ %		1.93	

4. Human-induced vibration response analysis

4.1 Experimental preparation for human-induced vibration

In order to obtain the maximum human-induced acceleration response in field tests, a total of nine test points was selected to place the accelerometers on the floor where the maximum response might appear from the mode shape results, as shown in Fig. 10. Two representative routes were selected: route 1 was along the longitudinal direction of the floor, and route 2 was along the transverse direction of the floor, similar to the FEM walking route in Fig. 14.

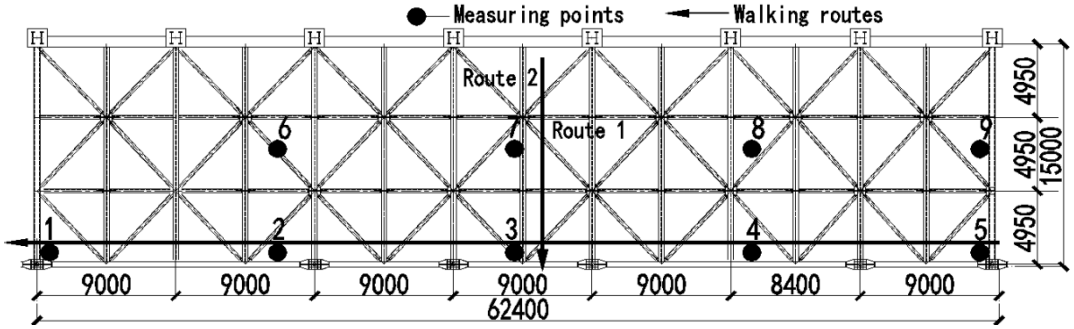

Fig. 10. Location of the accelerometers and two walking routes on the field test.

Then, the number of testers was determined referring to the walking density of the crowd. A quasi-free state of 0.385 pedestrians/m^2 was selected as the design factor based on the *American Road Traffic Capacity Manual HCM2000* and the practical function of the cantilevered floor. Finally, the maximum number of testers, 72 pedestrian, was determined (72 synchronized walking is equivalent to 360 pedestrian quasi-free walking, N~0.2n [36]), as shown in Fig. 11. Besides, the field tests of single, 20, and 40 pedestrian synchronized walking were conducted. Synchronized walking frequency, 1.68Hz (half of the first vertical frequency), was determined based on the existing walking frequency range and structure frequency. Metronome was used to guide pedestrian to walk in the same and specified pace rate both for single and crowd pedestrian (body weight range: 45–90 kg, mean value: 66 kg). The corresponding number of synchronized crowds under different walking densities was shown in Table 4.

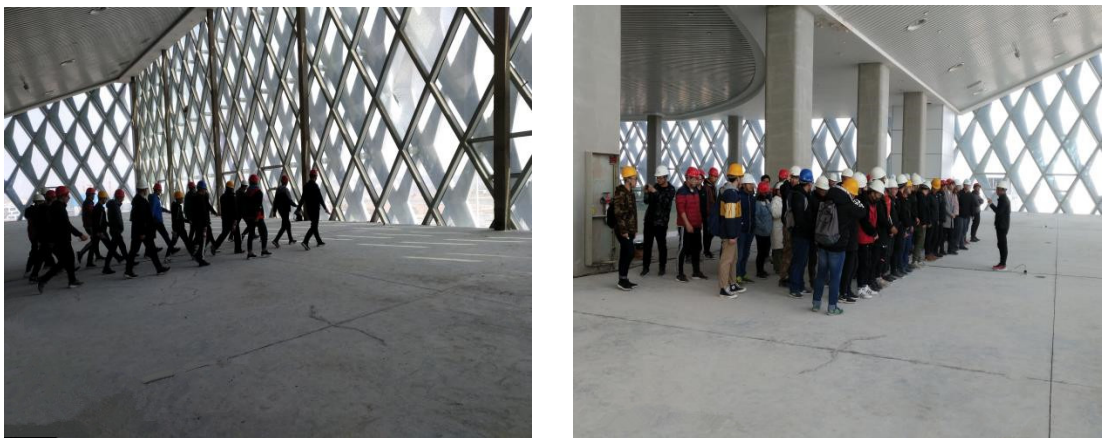

(a) (b)

Fig. 11. Field test: (a) 20 pedestrians walking (b) 72 pedestrians walking.

Table 4

The classes and density of pedestrian traffic

Description	Person per unit area (pedestrians/m^2)	Number of walkers (pedestrians)	Synchronized number (pedestrians)
Walking freely	0.106	100	20
	0.203	200	40
Quasi freely	0.385	360	72

4.2 Field test results for human-induced vibration analysis

Due to the limited space, the experimental results of route 2 excitation condition are shown and discussed here. Figs. 12–13 show the human-induced acceleration time history response of the floor FFT spectrum of the selected points (2, 3 and 7). It can be found that a significant sub-harmonics frequency component appears in the measured response. Furthermore, the FFT spectrum of test point 2 and 3 is mainly 3.4 Hz since it is located near the first vertical frequency, while the high frequency is the main frequency of test point 7 in the middle of the span. From the time domain curve, the acceleration response of the cantilevered floor is different from that of the ordinary floor, which is generally large in the middle and small on both sides because of the constraint condition. However, the response in the cantilevered floor tends to increase continually along the cantilevered direction. The acceleration response is up to the maximum at the point of the first vertical frequency peak. The results of all measured points are concluded in Table 5.

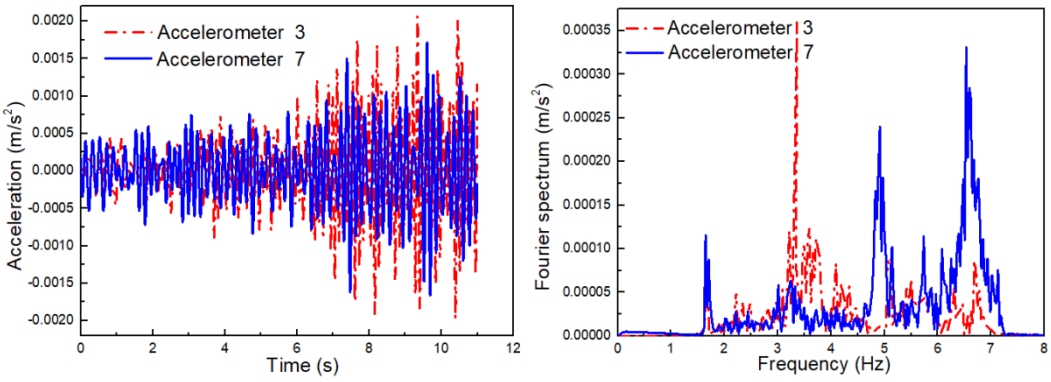

(a) (b)

Fig. 12. Acceleration time history and FFT spectrum of different measuring points for walking of a single pedestrian: (a) Acceleration time history (b) FFT spectrum.

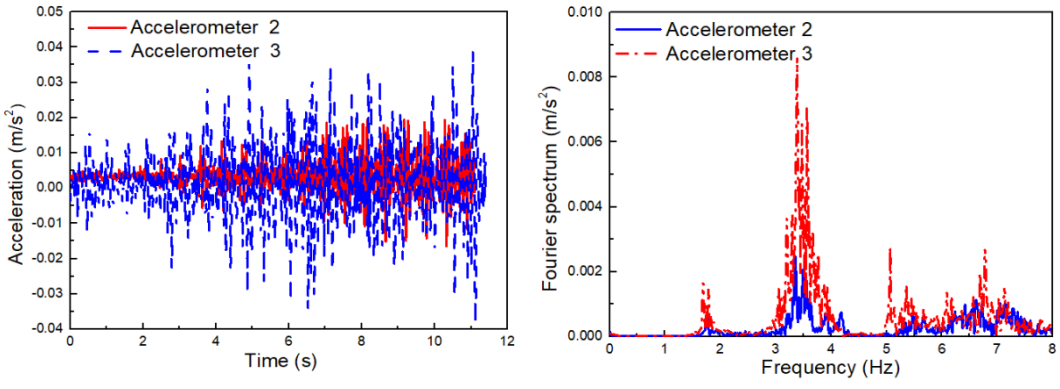

(a) (b)

Fig. 13. Acceleration time history and FFT spectrum of different measuring points for walking of 20 pedestrians: (a) Acceleration time history (b) FFT spectrum.

Table 5

Peak accelerations in different loading conditions of synchronously walking.

Number of	Acceleration response value of each channel (m/s^2)								
pedestrians	#1	#2	#3	#4	#5	#6	#7	#8	#9
1	0.0014	0.0008	0.0021	0.0006	0.0009	0.0005	0.0017	0.0004	0.0005
20	0.0149	0.0180	0.0400	0.0110	0.0160	0.0220	0.0380	0.0200	0.0250
40	0.0207	0.0200	0.0830	0.0320	0.0270	0.0480	0.0800	0.0580	0.0590

It was obvious that the peak acceleration of the floor under pedestrians' load was larger than that under a single pedestrian. Under synchronized walking excitation, the mean accelerations of single pedestrian, 20 and 40 pedestrians along Route 2 were 0.000983 m/s^2, 0.0228 m/s^2, and 0.0475 m/s^2, respectively. The largest displacement occurs in the measuring point #3 of the mode 1 which was mainly discussed in the following part. The peak acceleration of #3 for a single pedestrian was 0.0021 m/s^2 and 0.040 m/s^2 for 20 pedestrians which were 20 times of the former one. Similar result also occurred in the 40 pedestrians with the peak acceleration of 0.083 m/s^2.

The maximum allowable acceleration of structure has been restricted referring to Murray Specifications [34] for the operating rooms, offices, residential buildings, shopping malls, and restaurants. The cantilevered part was used for lounge; therefore, the maximum allowable vertical acceleration for the floor was 0.15 m/s^2. It can be seen that the maximum acceleration was 0.083 m/s^2 under the excitation of synchronous walking for the floor which is less than 0.15 m/s^2. Thus, the cantilevered floor can satisfy the requirement of the serviceability assessment standard.

4.3 Numerical vibration response without HSI

Since the pedestrian load was composed of main-harmonics and sub-harmonics, it was necessary to define the amplitude of them, respectively. It was a bit complicated, because the existence of energy spreading around the main-harmonics and sub-harmonics can be equivalent. For each of them, a sinusoidal load can be defined in such a way that its power is equal to the power of the analyzed harmonics. A coefficient can be obtained from the amplitude of this sinusoid divided by the subject's weight, which is commonly accepted for characterizing each load harmonics. This value is called the dynamic loading factor (DLF) [18].

For the i^{th} harmonic, occurring at frequency if_p, the main- harmonics could be obtained from the Eq. (1):

$$F_i(t) = \sum_{i=1}^{3} \alpha_i \sin(2\pi i f_p - \varphi_i) \tag{1}$$

While for the i^{th} sub-harmonics, it was expressed in Eq. (2)

$$F_i^s(t) = \sum_{i=1}^{3} \beta_i \sin(2\pi i f_p^s - \varphi_i^s) \tag{2}$$

where f_p was the walking pacing frequency (Hz); the power for each sub-harmonics f_p^s was calculated in the frequency range and it was more appropriate to be named as the sub-harmonic appearing at a frequency of $(i-0.5)f_p$; φ_i and φ_i^s was the phase angle which was based on a

uniform distribution of phases in the interval $[-\pi,+\pi]$; i was the sub-harmonics considered (i = 1,2,3…), and α_i is the dynamic loading factor; the DLFs for sub-harmonics β_i is considered as the function of DLF (α_i), i.e., $\beta_1 = 0.026\alpha_1 + 0.031$, $\beta_2 = 0.074\alpha_1 + 0.001$, $\beta_3 = 0.012\alpha_1 + 0.001$. Finally, the total force can be obtained by Eq. (3):

$$F(t) = \sum_{i=1}^{3} F_i(t) + \sum_{i=1}^{3} F_i^s(t) \tag{3}$$

In the numerical analysis, only the vertical pedestrian load was loaded into the structural FEM nodes according to the time sequence. However, the HSI was not considered when simulating a single pedestrian load and multiple pedestrians' load. As shown above, the first vertical frequency of the modified FEM was 3.37 Hz. Thus, the walk pacing frequency of 3.37/2 = 1.68 Hz was determined in the model and with a step length of 0.75 m. To make a comparison with experimental results, two routes were used: route 1 was the longitudinal direction of the floor, and route 2 was the lateral direction, as shown in Fig. 14. Each load route was set to pass through the peak point of the first mode (node number: #12554). Therefore, the maximum acceleration response in the numerical analysis occurred in node #12554 which was compared with the response of #3 (experimentally measured points) as shown in Figs. 15–17. The peak acceleration responses of the floor at the same position are listed in Table 6.

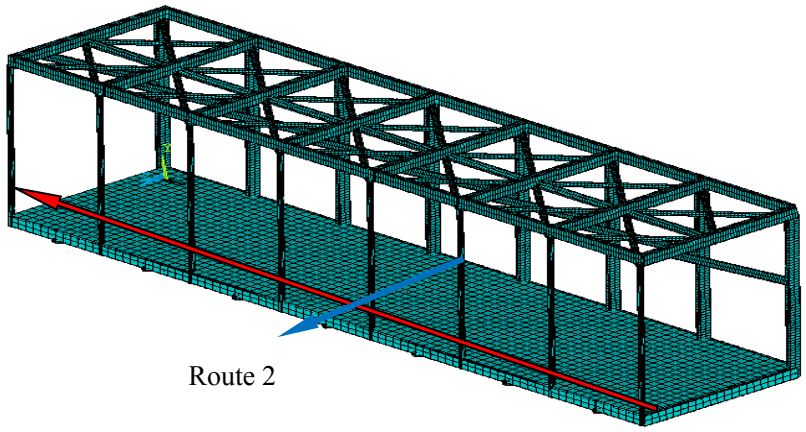

Fig. 14. Two walking routes on the test floor.

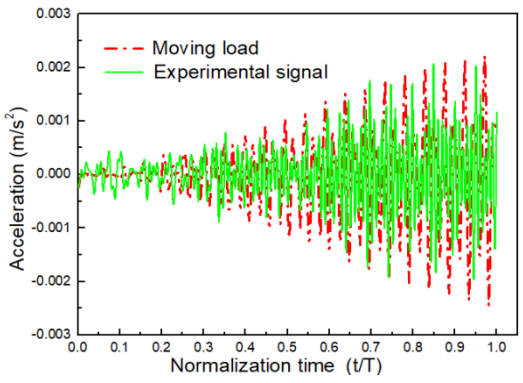

(a)

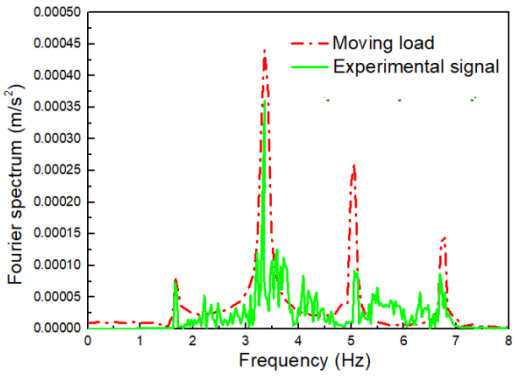

(b)

Fig. 15. Comparison of acceleration time history and FFT spectrum curve of walking of a single pedestrian between experimental and numerical (without HSI) results: (a) acceleration time history (b) FFT spectrum.

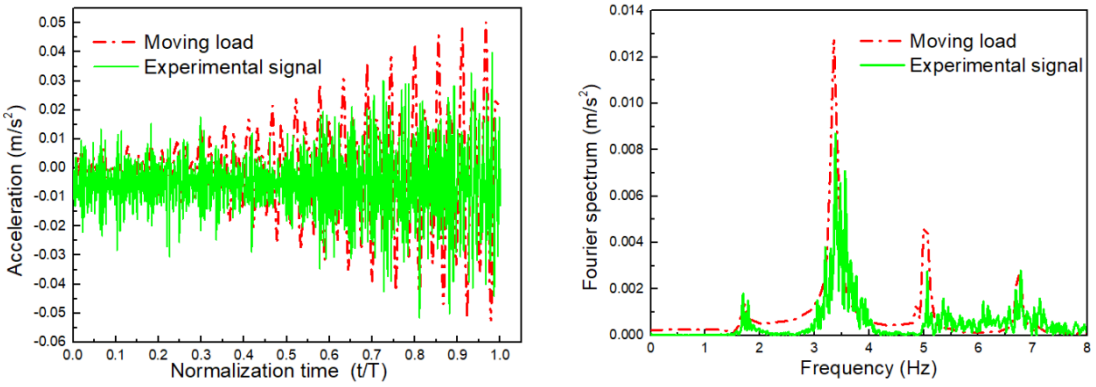

(a) (b)

Fig. 16. Comparison of acceleration time history and FFT spectrum curve of walking of 20 pedestrians between experimental and numerical (without HSI) results: (a) acceleration time history (b) FFT spectrum.

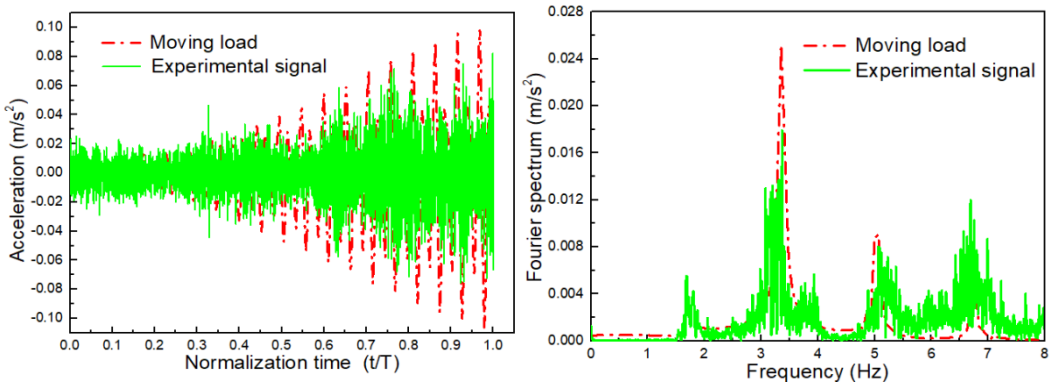

(a) (b)

Fig. 17. Comparison of acceleration time history and FFT spectrum curve of walking of 40 pedestrians between experimental and numerical (without HSI) results: (a) acceleration time history (b) FFT spectrum.

Table 6

Comparisons of experimental and numerical (without HSI) results of structural responses.

Number of walking pedestrians (pedestrian)	Vertical acceleration (m/s²)		
	Moving load (numerical)	Experiment	Error (%)
Single pedestrian walking synchronously	0.00222	0.00206	7.21
20 pedestrian walking synchronously	0.0504	0.0400	20.63
40 pedestrian walking synchronously	0.1003	0.0830	12.05
72 pedestrian walking synchronously	0.1233	0.1020	17.27

It can be seen from Figs. 15–17 that if the load model with main- harmonic and sub-harmonics components is applied by referring to Živanović [18] in the pedestrian load model, the spectrum of the FEM is closer to the measured. However, the acceleration time history without considering the human structure interaction is larger. Table 6 shows that the acceleration response induced by a single pedestrian was close under different conditions of considering the HSI or not. However, if the HSI was not considered, the peak acceleration of 20 pedestrians' load was 0.0504 m/s^2, which was 20.63% higher than the experimental result of 0.04 m/s^2. Similarly, the peak acceleration of 40 pedestrians' load without considering the HSI was 0.1003 m/s^2, which was 17.25% higher than the experimental result of 0.083 m/s^2, as shown in Table 6. Therefore, it can be concluded that only using a Fourier series load model to represent the pedestrian load leads to a large error compared with the experimental response in the structure.

4.4. Numerical vibration response with HSI

4.4.1 Biodynamic model of pedestrian for HSI

In order to consider the coupling human-structure vibration, a single-degree-of-freedom (SDOF) biodynamic model was employed in this section, as shown in Fig. 18. Among them, m_p, k_p, and c_p represent the mass, stiffness, and damping of the human body, respectively. F_t represents the pedestrian load, u_p represents the pedestrian vertical displacement and u represents the vertical displacement of the cantilevered floor.

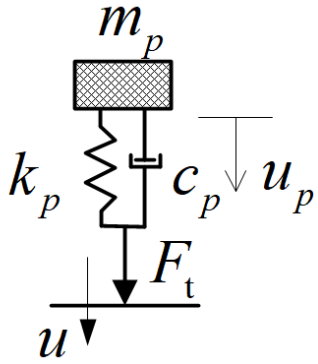

Fig. 18. Single-degree-of-freedom biodynamic model.

The regression expression of human parameters can be expressed as the function of body weight M and pedestrian walking frequency f_p, as shown in Eqs. (4–6) [25].

$$m_p = 97.082 + 0.275M - 37.518 f_p \tag{4}$$

$$c_p = 29.041 m_p^{0.883} \tag{5}$$

$$k_p = 30351.744 - 50.261 c_p + 0.035 c_p^2 \tag{6}$$

4.4.2 Comparisons of experimental and numerical vibration responses with and without HSI

When considering the interaction between human and structure, the established SDOF biodynamic model was used combined with the Fourier series load model to represent the

pedestrian load in FEM and the movable pedestrian load was realized in FEM by the deactivation elements when pedestrian were walking along the routes.

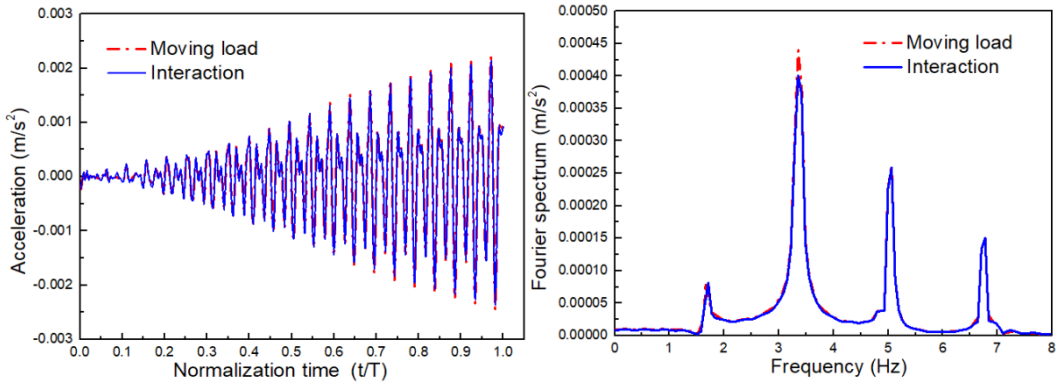

(a) (b)

Fig. 19. Comparison of acceleration time history and FFT spectrum curve of walking of a single pedestrian (with and without HSI) in the numerical: (a) acceleration time history (b) FFT spectrum.

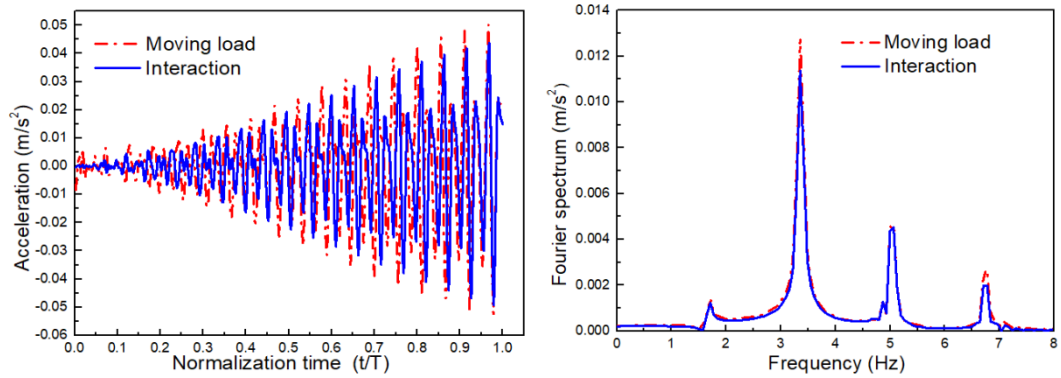

(a) (b)

Fig. 20. Comparison of acceleration time history and FFT spectrum curve of walking of 20 pedestrians (with and without HSI) in the numerical: (a) acceleration time history (b) FFT spectrum.

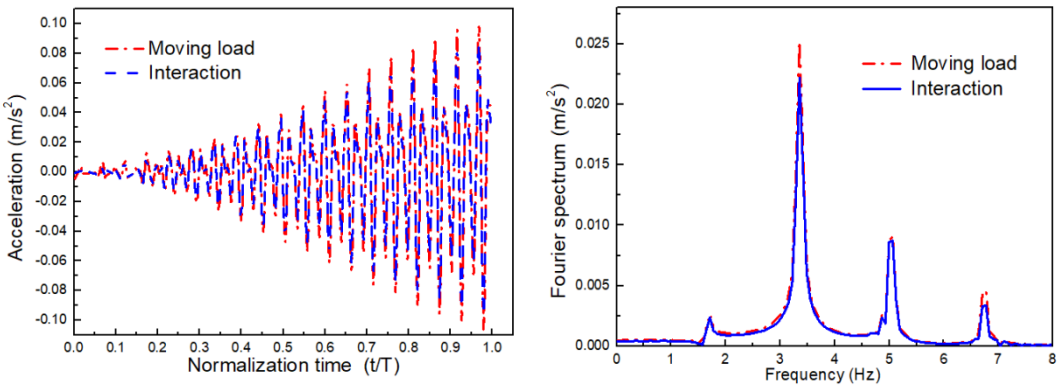

(a) (b)

Fig. 21. Comparison of acceleration time history and FFT spectrum curve of walking of 40

pedestrians (with and without HSI) in the numerical: (a) acceleration time history (b) FFT spectrum.

Table 7

Acceleration comparison among numerical with and without HIS and experiment in different walking conditions.

Number of walking pedestrians (pedestrian)	Vertical acceleration (m/s^2)		
	Moving load	Interaction	Experimental signal
Single walking synchronously	0.00222	0.00213	0.00206
20 pedestrian walking synchronously	0.0504	0.0437	0.0400
40 pedestrian walking synchronously	0.1003	0.0865	0.0830
72 pedestrian walking synchronously	0.1233	0.1083	0.1020

Figs. 19–21 show the comparison of acceleration time history curves and FFT spectrum with versus without considering HSI. Acceleration comparison among FEM with and without HSI and experiment in different walking conditions are listed in Table 7. It can be seen that the peak acceleration of the floor decreased when the HSI was considered. Among them, when 20 pedestrians walked synchronously, the peak value of the HSI acceleration was 0.0437 m/s^2, which was 13.29% lower than that without considering the HSI acceleration (0.0504 m/s^2). The peak acceleration of the synchronous walking of 40 pedestrians was 0.0865 m/s^2, which was 13.76% lower than that without considering the interaction (0.1003 m/s^2). Considering the HSI under the pedestrians' load, the effect on the vibration response of the structure is obvious, whereby the results are consistent with the literature [6, 14]: if the interaction between pedestrian and structure is neglected, the dynamic response of the structure will be overestimated compared with the experimental results. Therefore, the establishment of the human biomechanical model is of great significance to further explore the pedestrian-structure dynamic interaction.

Finally, a comprehensive comparison of the acceleration time history and FFT spectrum was compared regarding Fourier series loading model and the biomechanical model of the floor simulated in the FEM and experiments as shown in Figs. 22–24, respectively. The peak accelerations of the floor of the same point in three cases are listed in Table 8.

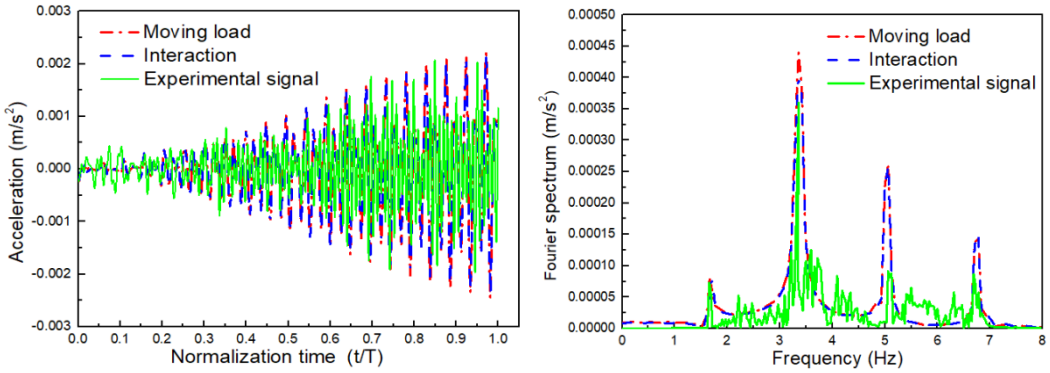

(a) (b)

Fig. 22. Comparison of acceleration time history and FFT spectrum curve of walking of a single pedestrian: (a) Acceleration time history (b) FFT spectrum.

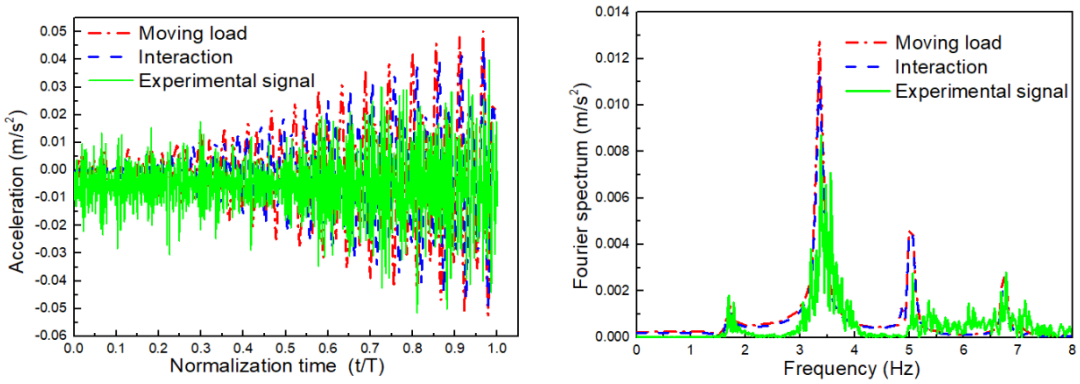

(a) (b)

Fig. 23. Comparison of acceleration time history and FFT spectrum curve of walking of 20 pedestrians: (a) Acceleration time history (b) FFT spectrum.

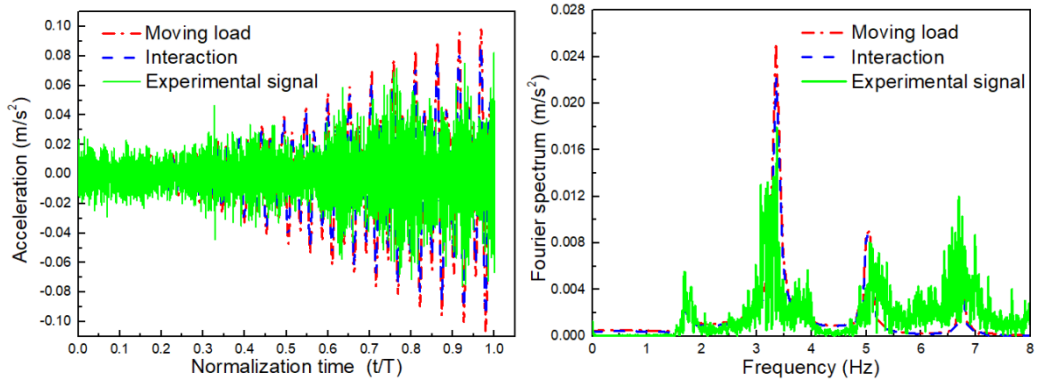

(a) (b)

Fig. 24. Comparison of acceleration time history and FFT spectrum curve of walking of 40 pedestrians: (a) Acceleration time history (b) FFT spectrum.

Table 8

Comparisons of experimental and numerical results of human-induced vibration.

Number of walking pedestrians (pedestrian)	Vertical acceleration (m/s²)			
	Moving load	Interaction	Experimental	Error between interaction and experimental (%)
Single pedestrian	0.00222	0.00213	0.00206	3.28%
20 pedestrians	0.0504	0.0437	0.0400	8.47%
40 pedestrians	0.1003	0.0865	0.0830	4.05%
72 pedestrians	0.1233	0.1083	0.1020	5.82%

Table 8 shows that the peak acceleration of walking of 20 pedestrians considering the HSI was 0.0437 m/s², which gives an 8.47% deviation compared with the measured peak acceleration of 0.04 m/s². The peak acceleration of walking of 40 pedestrians considering the HSI was 0.0865 m/s² with 4.05% error compared with the measured peak acceleration of 0.083 m/s².

Therefore, the acceleration response of human-induced vibration calculated by the FEM cannot agree well with the measured results because the HSI was not considered in the FEM only with

Fourier series load. The biomechanical model equivalent to the crowd load with main-harmonics and sub-harmonics components is closer to the experimental results. The reliability of the biomechanical model is further confirmed. The results further indicate that the human-structure coupling vibration is essential for serviceability assessment.

5. Discussion

In this paper, the weak constraint effect was proposed for the curtain wall acting as a non-structural component. Then, the FEM was updated by considering the contribution of the curtain wall to floor stiffness. The results obtained from the updated FEM vibration mode was in excellent agreement with the experimental results. The weak constraint effect of glass curtain walls was proposed based on the existing specification [34]. Increasing the frequency and mode of the floor by providing stiffness contribution for non-structural components was presented. However, a large number of theoretical and experimental studies are still needed on the weak constraint effect of the glass curtain wall and its quantitative formula of stiffness.

When simulating the HSI, the structural damping ratio was selected according to the damping ratio of the floor under ambient excitation and calculated according to the same damping ratio. Existing studies show that the damping ratio of the structure is related to the amplitude of the floor, and the damping ratios of the floor under the action of a person will be different as opposed to that of multiple pedestrians [37]. Therefore, the structural damping ratio needs to be further studied and analyzed to obtain the damping ratio suitable for the FEM of the floor.

The gait cycle will change from 3% to 4% in the course of walking. Even under the control of the metronome, the gait cycle will change while the change range will be rather small [38]. For the walking frequency of the crowd, this paper simplifies the loading according to the same step frequency. However, more accurate FEMs should take frequency variations into account.

For single person walking, there is little difference between the acceleration with and without HSI, only 4.05%, while for the crowd, HSI cannot be ignored, such as 20 and 40 pedestrians, the difference is 13.29% and 13.76%, respectively. However, The MSD model we proposed in this paper, needs further verification and improvement by referring to the existing narrow band model of Živanović [18], the inter-subject variability, such as walking frequencies, force amplitudes, and step lengths need to be further studied for better agreement between numerical analysis and experimental.

6. Conclusions

In this paper, the experimental investigation and numerical analysis on structural vibration mode and responses were conducted. The FEM for the whole structure was updated comparing with the field test based on the effect of weak constraint of glass curtain walls. The human-induced vibration was systematically analyzed, whose results were compared with those from field tests, confirming the significance of HSI. The structural serviceability was evaluated experimentally and numerically to provide reference for the human-induced vibration analysis. Several important conclusions are summarized as follows.

(1) By comparing with the field test for structural vibration modes, the FEM was updated by addressing the effects of non-structural components (the glass curtain wall), and showed that it had an effect on the structural vibration characteristics. Neglecting the weak constraint effect of glass curtain walls for the mode and vibration serviceability may lead to conservative design results.

(2) By comparing the numerical results of human-induced acceleration responses with and without HSI, the latter case overestimated the structural response. For example, when 20, 40, and 72 pedestrians walked synchronously, the peak accelerations considering the HSI were 13.29%, 13.76%, and 12.16%, less than that without considering the interaction, respectively. Thus, considering the HSI led to different results for acceleration responses.

(3) By comparing the structural responses under the Fourier series load and MSD model with the field test results respectively, it was demonstrated that the results from FEM analysis considering the HSI and sub-harmonics component was in good agreement with the experimental results. For example, the peak acceleration of walking of 20 pedestrians without considering the HSI was 0.0504 m/s^2, which was 20.63% higher than the measured peak acceleration (0.04 m/s^2), while the peak acceleration of walking of 20 pedestrians considering the HSI was 0.0437 m/s^2, which was 8.47% higher than the measured peak acceleration. Therefore, in order to obtain a more accurate human-induced vibration serviceability evolution in FEM analysis, the HSI and sub-harmonics components should be considered.

Acknowledgments

This work was supported by the National Natural Science Foundation of China (No. 51668042, 51868046, and 51508257) and the China Scholarship Council (No. 201808620022).

References

[1] Zheng X, Brownjohn, JMW. Modeling and simulation of human-floor system under vertical vibration //Smart Structures and Materials 2001: Smart Structures and Integrated Systems. International Society for Optics and Photonics, 2001, 4327: 513-520.

[2] Pavic A, Reynolds P. Vibration serviceability of long-span concrete building floors. Part 1: Review of background information. Shock and Vibration Digest, 2002, 34(3): 191-211.

[3] Drygala I J, Dulinska J M. A theoretical and experimental evaluation of the modal properties of a cable-stayed footbridge. Procedia Engineering, 2017, 199: 2937-2942.

[4] Devin, A, Fanning P J, Pavic A. Modelling effect of non-structural partitions on floor modal properties. Engineering Structures，2015，91：58-69.

[5] Setareh M.Vibration Serviceability of a Building Floor Structure. I: Dynamic Testing and Computer Modeling. Journal of Performance of Constructed Facilities，2010，24(6)：497-507.

[6] Salyards K A, Noss N C. Experimental evaluation of the influence of human-structure interaction for vibration serviceability. Journal of Performance of Constructed Facilities, 2013, 28(3): 458-465.

[7] Petrovic S, Pavic A. Effects of non-structural partitions on vibration performance of floor structures: A Literature Review//Int. Conf. Struct. Dyn.(EURODYN 2011), Leuven, Belgium. 2011.

[8] Miskovic Z, Pavic A, Reynolds P. Effects of full-height nonstructural partitions on modal properties of two nominally identical building floors. Canadian journal of civil engineering, 2009, 36(7): 1121-1132.

[9] Jarnerö K., Brandt A., Olsson A. Vibration properties of a timber floor assessed in laboratory and during construction. Engineering structures, 2015, 82: 44-54.

[10] Rijal R, Samali B, Shrestha R, et al. Experimental and analytical study on dynamic performance of timber floor modules (timber beams). Construction and Building Materials, 2016, 122: 391-399.

[11] Chen J, Yan S, Zhang M. Vibration performance assessment of a long-span concrete floor using field measurements over a five-year period. Advances in Structural Engineering, 2014, 17(8): 1145-1158.

[12] Fanning P J, Devin,A. Vibration Transmission Through Non-Structural Partitions Between Building Floor Levels//Dynamics of Civil Structures, Volume 2. Springer, Cham, 2016: 297-302.

[13] Pavic A, Widjaja T, Reynolds P. The use of modal testing and FE model updating to investigate vibration transmission between two nominally identical building floors//Proc., Int. Conf. on Structural Dynamics Modeling-Test, Analysis, Correlation and Validation. Lisbon, Portugal: Instituto Superior Tecnico, 2002: 347-355.

[14] Ellis B R, Ji T, BRE. Human-structure interaction in vertical vibrations. Proceedings of the Institution of Civil Engineers-Structures and Buildings, 1997, 122(1): 1-9.

[15] Zhu Q K, Hui X L, Nan N N, et al. Study on the Vertical Dynamic Coupled Effects of the Crowd-structure System based on the Social Force Model. KSCE Journal of Civil Engineering. 2019,23(5):2243-2253

[16] Feldmann M, Heinemeyer C, Lukic M. Design of Footbridges. Guideline. Human Induced Vibrations of Steel Structure (Hivoss). 2008.

[17] Steel B S I. concrete and composite bridges. Specification for loads, BS 5400: Part 2. British Standard Institution, 1978.

[18] Živanović S, Pavić A, Reynolds P. Probability-based prediction of multi-mode vibration response to walking excitation. Engineering Structures, 2007, 29(6): 942-954.

[19] Brownjohn J M W, Pavic A, Omenzetter P. A spectral density approach for modelling co ntinuous vertical forces on pedestrian structures due to walking. Canadian Journal of Civil Engineering, 2004, 31(1): 65-77.

[20] Živanović S, Pavic A, ReynoldsP. Human–structure dynamic interaction in footbridges//Pro ceedings of the Institution of Civil Engineers-Bridge Engineering. Thomas Telford Ltd, 20 05, 158(4):165-177.

[21] Sachse R, Pavic A, Reynolds P. The influence of a group of humans on modal properties of a structure//Proceedings of the fourth international conference on structural dynamics. 2002, 2: 1241-1246.

[22] Barker C, Mackenzie D. Design methodology for pedestrian induced footbridge vibrations. Proceedings of footbridge, 2008.

[23] Lenzen K H. Vibration of steel joist-concrete slab floors. AISC. Eng. Jour., 1966, 3: 133-136.

[24] Kim S H, Cho K I, Choi M S, et al. Development of human body model for the dynamic analysis of footbridges under pedestrian induced excitation. Steel Structures, 2008, 8: 333—345.

[25] Silva F T, Pimentel R L. Biodynamic walking model for vibration serviceability of footbridges in vertical direction//Proceeding of the 8th International Conference on Structural Dynamics (Eurodyn'11). 2011: 1090-1096.

[26] Da Silva F T, Brito H M B F, Pimentel R L. Modeling of crowd load in vertical direction using biodynamic model for pedestrians crossing footbridges. Canadian Journal of Civil Engineering, 2013, 40(12): 1196-1204.

[27] Dang H V, Zivanovic S. Modelling pedestrian interaction with perceptibly vibrating footbri dges．FEM Transactions，2013,41(4):271-278

[28] Gheitasi A, Ozbulut O E, Usmani S, et al. Experimental and analytical vibration serviceability assessment of an in-service footbridge. Case Studies in Nondestructive Testing and Evaluation,

2016, 6: 79-88.

[29] Živanović S, Díaz I M, Pavić A. Influence of walking and standing crowds on structural dynamic properties. Proceedings of IMAC-XXVII, Orlando, 2009: 9-12.

[30] Lai E, Gentile C, Mulas M G. Experimental and numerical serviceability assessment of a steel cantilever footbridge. Journal of Constructional Steel Research, 2017, 132: 16-28.

[31] Cao L, Liu J, Li J, et al. Experimental and analytical studies on the vibration serviceability of long-span prestressed concrete floor. Earthquake Engineering and Engineering Vibration, 2018, 17(2): 417-428.,

[32] Wang,D., Wu C, Zhang Y, et al. Study on vertical vibration control of long-span steel footbridge with tuned mass dampers under pedestrian excitation. Journal of Constructional Steel Research, 2019, 154: 84-98.

[33] Chen J, Liu Q, She X. Field measurements and assessment of vibration serviceability of as-built long-span concrete floor. International Journal of Structural Engineering, 2012, 3(1-2): 61-74

[34] Murray T M, Allen D E, Ungar E E, et al. Vibrations of steel-framed structural systems due to human activity. American Institute of Steel Construction, 2016.

[35] Zhu Q K, Hui X L, Du Y F, et al. A full path assessment approach for vibration serviceability and vibration control of footbridge. Structural Engineering and Mechanics. 2019,70(6):765-779

[36] Fujino Y, Pacheco B M, Nakamura S I, et al. Synchronization of human walking observed during lateral vibration of a congested pedestrian bridge. Earthquake Engineering and Structural Dynamics, 1993, 22(9):741-758.

[37] Živanović S, Díaz I M, Pavić A. Influence of walking and standing crowds on structural dynamic properties//Proceeding of Conference & Exposition on Structural Dynamics (IMAC XXVII). 2009.

[38] Scafetta N, Marchi D, West B J. Understanding the complexity of human gait dynamics. Chaos: An Interdisciplinary Journal of Nonlinear Science, 2009, 19(2): 026108.

Declaration of interests

 The authors declare that they have no known competing financial interests or personal relationships that could have appeared to influence the work reported in this paper.

The authors declare the following financial interests/personal relationships which may be considered as potential competing interests:

Author statement

Authors listed in this manuscript have made contributions to the reported work. Qian-kun Zhu was responsible for the conceptualization and design of the whole work. Kai-fang Liu conducted the FE analysis, field tests, data analysis and wrote the original manuscript under the guidance of Qian-kun Zhu. Yong-feng Du organized 72 people for the tests and supervised the field tests. Other two authors Lu-lu Liu and Stana Zivanovic were responsible for revising the manuscript, including grammar and writing.

Experimental and numerical analysis on serviceability of cantilevered-floor based on human-structure-interaction

Qiankun Zhu*[1,2a], Kaifang Liu[1b], Lulu Liu[3a], Yongfeng Du[1c], Stana Zivanovic[2b]

[1]*Institute of Earthquake Protection and Disaster Mitigation, Lanzhou University of Technology, Lanzhou, Langongping Road 287, 730050, China*

[2]*College of Engineering, Mathematics and Physical Science, University of Exeter, North Park Road, EX4 4QF Exeter, UK*

[3]*College of Civil Engineering, Southeast University, Nanjing 211189, China*

Abstract: To evaluate the vibration serviceability of structure under human-induced excitation, experimental and numerical analysis on a cantilevered floor of a gymnasium assumed as a case study were conducted. A series of field tests were performed including the floor vibration mode measurement by the ambient excitation approach and the human-induced vibration response. Finite element (FE) models of the cantilevered floor were established, modified and validated first according to the field test mode and the weak constraint effect of glass curtain wall proposed in this paper. The numerical dynamic vibration responses induced by human were analyzed using the Fourier series load model combining with the Spring-Mass-Damper (SMD) human dynamic model as a single pedestrian load. To simulate the human-structure interaction (HSI) well, both the main harmonics and sub-harmonics load spectrum were considered for the equivalent load model because of the characteristics of narrow band. The experimental and numerical results were compared and agreed well in both structural vibration modes and human-induced acceleration responses. The weak constraint effect of glass curtain wall was validated. The numerical results were more accurate when considering the influence of the HSI on the structural vibration serviceability analysis in practical engineering applications.

Keywords: Cantilevered floor; Human-structure interaction; Field tests; FE modeling; Vibration serviceability; Weak constraint effect of glass curtain wall; Sub-harmonics components.

1. Introduction

With the increasing popularity of high-strength and light-weight materials, large-space structures, such as large-span cantilevered structures as a typical form of complex-space structures, have been widely used in public buildings. Long-span structures usually have characteristics of flexibility, slenderness, and low natural frequency. This frequency is close to the main band of low-frequency dynamic loads such as pedestrian excitation, therefore the dynamic response of the structure under such loads is significant, and its vibration serviceability issue is extremely prominent. Therefore, apart from the basic design requirement of ultimate limit state and serviceability limit state, human-induced vibration has become more critical in structural design, especially for large-span floors [1, 2, 3].

Obtaining structural mode shape and fundamental frequency accurately is the basic requirement for the numerical analysis of the structural vibration serviceability evaluation. Previous studies have indicated that the presence of non-structural members, such as decorative floors and glass curtain walls, affect the vibration characteristics of the floor. Devin et al. [4] concluded that non-structural members increased floor stiffness and significantly changed natural

*Corresponding author, Professor, E-mail: zhuqklut@qq.com

frequencies and vibration modes. After installing inner partitions, the natural frequencies increased by 30% compared with that of the bare state. [5, 6, 7, 8, 9, 10, 11] also had the similar conclusions that structural vibration mode was changed after the installation of some non-structural members and inner walls. Fanning et al. [12] and Pavic et al. [13] experimentally and numerically evaluated the effects of the non-structural partition on the vibration of multi-story concrete buildings and found that the floor vibration was caused by its inherent excitation, and some insignificant level of vibration transmitted through structural and non-structural components due to the simultaneous activity from floors between above and below. The curtain wall, as a non-structural component which always has a space system consisted of glass, skeleton and row-columns and provides a boundary condition for the floor. The effect of glass curtain wall on the vibration characteristics is also equivalent as additional mass and stiffness applied into the floor [4]. However, the calculated modal characteristics of the floor based on the existing equivalent method of the glass curtain wall were not in good agreement with the experimental results. Thus, the improved equivalent approach should be developed to consider the constraint effect of the glass curtain wall on the floor".

The numerical human-induced vibration can be realized by considering the pedestrian load as a Fourier series load model and applying it to the structure [14, 15, 16, 17]. Živanović et al. [18] concluded that sub-harmonics spectrum between the main harmonics could not be ignored which affected the pedestrian load based on the data analysis measured by Brownjohn et al. [19] and revised the Fourier load model. Later, some studies found that human occupied in the structure also had effects on the structural vibration frequency and damping, even the vibration responses and concluded that there existed HSI in the practical structure [20, 21, 22, 23]. Hence, the HSI should not be ignored in numerical analysis. Kim et al. [24] employed a biomechanical model to evaluate the HSI for a single pedestrian and showed that it was in good agreement with the experiment. Based on the measured acceleration of 20 pedestrians' walking on the stiff ground, Silva [25] proposed a single-degree-of-freedom human body dynamic model to simulate the vertical dynamic characteristics of pedestrian and structure. The mass, stiffness, and damping of the model were expressed by human body weight and walking frequency. Da et al. [26] and Dang [27] researched the vertical dynamic HSI based on the human body dynamic model. However, the effect of pedestrians on dynamic characteristics of the structure was not discussed in depth. Thus, besides employing the Fourier series load model to represent the pedestrian load, the sub-harmonics spectrum, a single-degree-of-freedom of mass-spring-damper system should also be developed to characterize the HSI for the numerical vibration analysis.

Currently, numerous studies have been done experimentally and numerically on the human-induced vibration and structural serviceability evaluation, such as footbridge, large-span floor [28, 29, 30, 31, 32, 33]. However, they cannot provide a complete analysis for the human-induced vibration based on the HSI and non-structural contribution. Limited research has investigated the vibration response of the cantilevered floor; it is different from the ordinary floor that generally has maximum deformation and response in the middle area of floor and minimum in both sides because of the boundary condition around the floor. The maximum deformation and response of the cantilevered floor occurs often in the end of cantilever structure. Thus, detailed studies are still necessary to experimentally and numerically investigate the influence of human-induced vibration on the floor considering the HSI and the non-structural effects.

The outline of this paper is as follows: Section 2 gave a brief description of the Gymnasium

building, including the characteristic of structural elements and floor. Section3 presented the experimental mode of the floor and updated the FE model based on the proposed weak constraint effect of glass curtain wall. Section 4 conducted the acceleration field test on the floor under pedestrians' load, and the sub-harmonics in the force spectrum were explained. Then, we provided a brief discussion of the acceleration response between FE results and measurements from field tests, and highlighted the impact of HSI on the vibration serviceability evaluation of structures. Finally, the main discussions and conclusions were summarized in Sections 5 and 6, respectively.

2. Structural basic information

The Gymnasium is located in the Northwest of China, with a total construction area of 51800 m^2. According to the functional requirements of the building, the steel truss of the Gymnasium includes the main truss and suspension structures (cantilevered overhead the truss), consisting of a competition hall and a training hall. The investigated cantilevered floor was part structure of a Gymnasium overhanging 15.0 m at an elevation of 13.5 m as shown in Fig.1, whose main function is the lounge; as a gathering place for personnel, it provides people with rest and exhibits.

(a) (b)

Fig. 1. Front view (a) and left view (b) of the cantilevered floor structure under construction.

The cantilevered structure adopts a steel frame-support structure. The column supported the whole structure, and truss is steel reinforced concrete (SRC) material. Box-type and H-type steel beams are employed, and the upper steel beam has a diagonal brace. The floors between the trusses are connected by pillars and slings at the cantilevered end, which are the main load-bearing elements in the cantilevered end. The steel truss deck as a new structural type is used in the floor system, with a thickness of 180 mm. In order to meet the requirements of architectural design for permeability and lighting, a large-span glass curtain wall is set around the 15-meter suspended lounge on the East side. The section of the whole Gymnasium and plan of the cantilevered truss are shown in Fig. 2. Its main floor components are listed in Table 1.

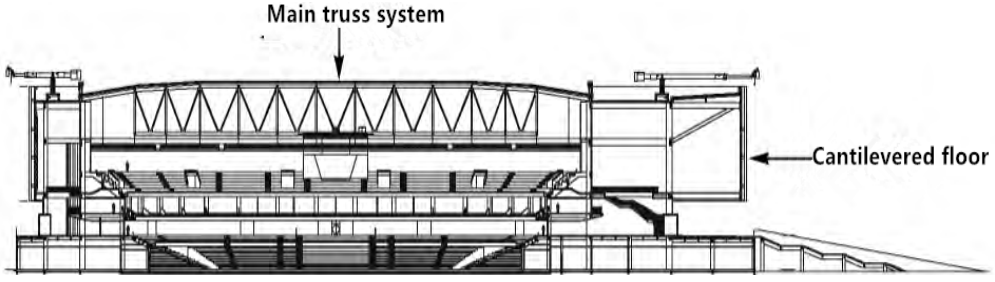

(a)

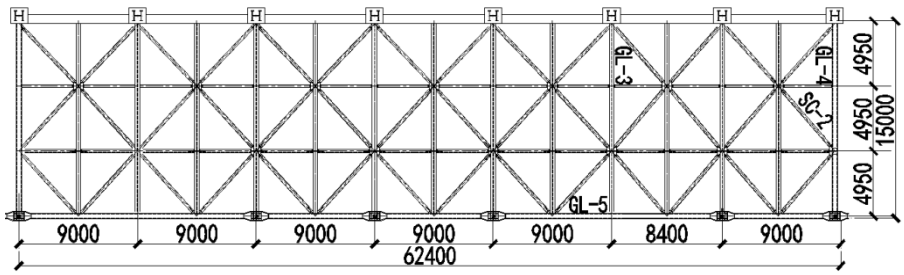

(b)

Fig. 2. Section (a) and plan (b) of the building.

Table 1

Parameters of cantilevered floor members

Member items	Sectional specification	Section type	Remarks
GL3	H1000×350×20×24	Welding H shape	secondary-beam
GL4	B1000×400×20×24	Welding rectangle	secondary-beam
GL5	B1000×400×20×24	Welding rectangle	main-beam
SC2	P 245×8.0	Hot rolling seamless	Horizontal support

3. Modal analysis for the cantilevered floor

3.1 Field test preparation

The ambient excitation test was conducted on the cantilevered floor to obtain the dynamic properties of the gym and verify the FE model. Limited modal testing was conducted when the whole structure was completed but not open to the public. As the floor vibration test is greatly influenced by the external environment, the test time is selected at night to eliminate the interference from vehicles and other external factors. Thus, the ideal natural pulsation signal was measured. The field test is shown in Fig. 3, and the modal tests were performed using a 941B accelerometer and INV3060V acquisition system.

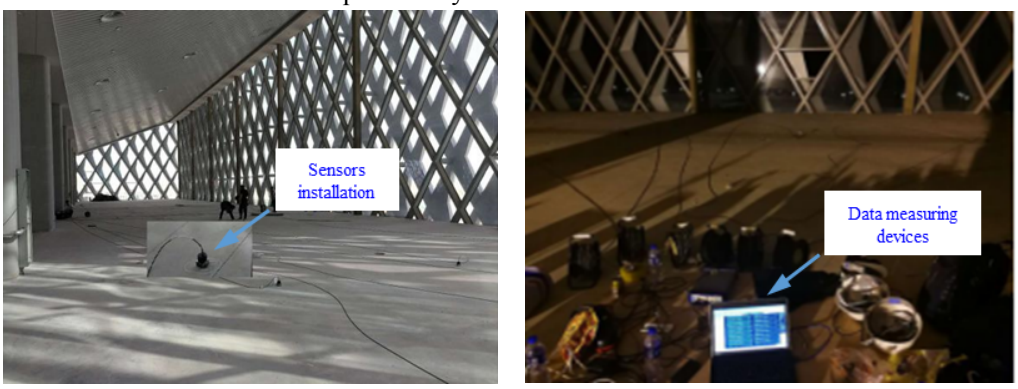

(a) (b)

Fig. 3. Field test: (a) Installation of the accelerometers (b) Data measuring devices.

85 test points in totally were selected in this test for placing accelerometers to accurately map mode shapes. As the existing equipment cannot complete the data collection of all measuring points at one time, we collected the data for multiple times by moving the test points. In order to identify multiple sets of data together, the #76 was selected as the reference point and collected at each test; #1, #6, #11, #16, #21, #26, #31 and #36 were the first test points totally moved along the main beam ten test cases, as shown in Fig. 4. The sampling frequency was 256 Hz, and corresponding recording times were all 15 minutes for each setup.

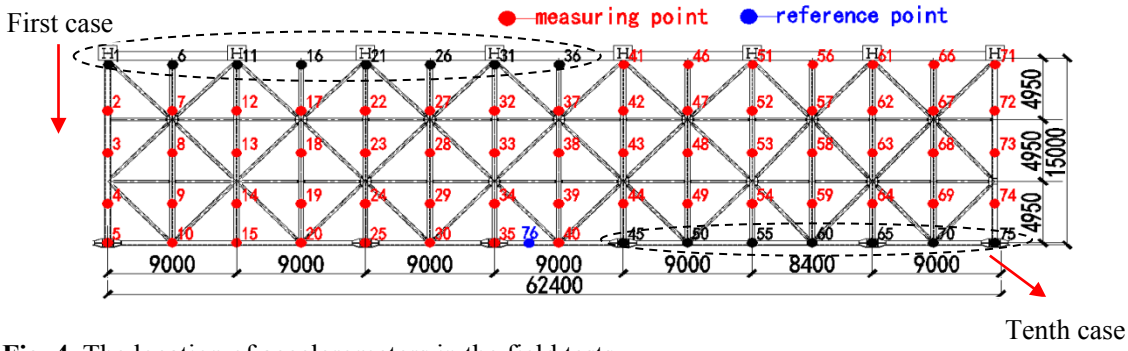

Fig. 4. The location of accelerometers in the field tests.

3.2 Field test results for mode shapes

The Stochastic Subspace Identification (SSI) approach was used to process the data. The frequencies of six vibration modes were obtained directly as follows: 3.36, 4.13, 5.23, 6.63, 7.38, and 8.08 Hz, respectively. The experimental vibration modes are shown in Fig. 5. It could be concluded that the fundamental frequency of the structure meets the requirement of the code of AISC Design Guide 11 (Murray et al. 2016) [34]: Large-span public buildings should not be less than 3 Hz. As the first vertical frequency was still rather low, the vibration serviceability evaluation was conducted in the following parts.

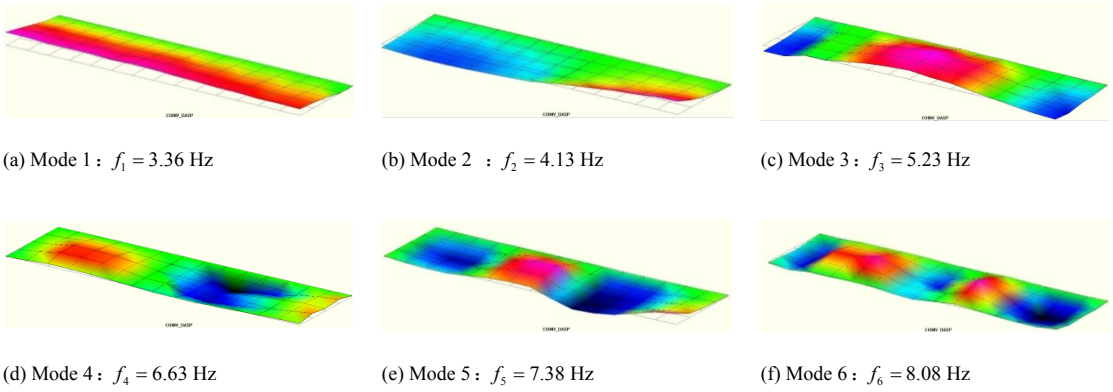

(a) Mode 1： $f_1 = 3.36$ Hz (b) Mode 2 ： $f_2 = 4.13$ Hz (c) Mode 3： $f_3 = 5.23$ Hz

(d) Mode 4： $f_4 = 6.63$ Hz (e) Mode 5： $f_5 = 7.38$ Hz (f) Mode 6： $f_6 = 8.08$ Hz

Fig. 5. Natural frequencies and mode shapes determined by the SSI approach.

3.3 Numerical analysis for mode shapes

3.3.1 FE model of the cantilevered floor

APDL language was used in ANSYS to input component parameters, material properties, select the element type, establish the model and obtain the results. In this study, BEAM188 element (a kind of 3D linear elements) was used to simulate the steel truss, the cantilevered column, and the steel beam at the bottom of the slab, whose Young's modulus, density, and PRXY is $2e^{11}$ N/mm, 7850 kg/m^{3}and 0.3, respectively; SHELL181 element was selected to model the concrete slab, whose Young's modulus, density, and PRXY is $3.15e^{10}$ N/mm, 2550 kg/m^3, and 0.2, respectively; while LINK180 element was employed to simulate the slings, web bars, and struts. Due to the complexity of the glass curtain wall system, MASS21 element was chosen to simplify the simulation of the glass curtain wall, In the FE model, each component was modeled by its own node; different components all have coincident nodes at the same location; the connection between different components of the overall structure was achieved by merging nodes at the same location; after merging, only one node was contained in the same location, as shown in Figs. 6(a)–

(b).

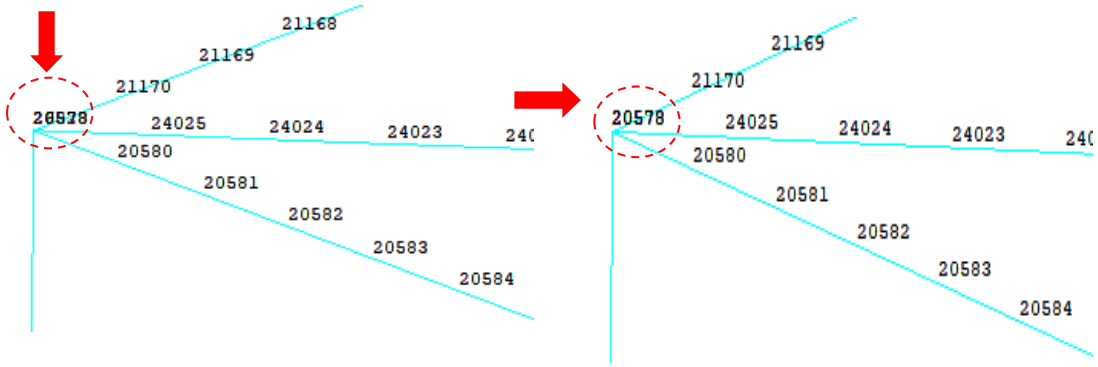

(a) (b)

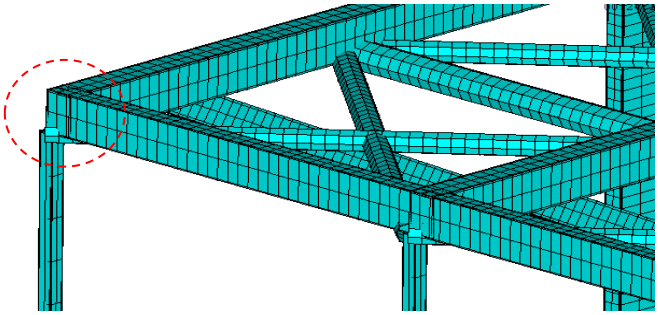

(c)

Fig. 6. Merging different components: (a) before merge (b) after merge (c) size shape of different components.

Finally, a reasonable simulation of boundary conditions is the key to obtain dynamic response analysis. In the practical structure, the constraint between beams and columns is a semi-rigid constraint between hinge and fixed condition. In this paper, spring elements were used to simulate this constraint state. Considering the vibration modal of the cantilevered floor, the constraint condition was defined as below, the translational freedoms UXYZ except UZ and the rotational freedom were fixed, release the axial constraint UZ between beams and columns; the axial spring damper COMBIN14 was used to further simulate the slip between beams and columns, thus achieving the semi-rigid condition, as shown in Figs. 7(b)–(c).

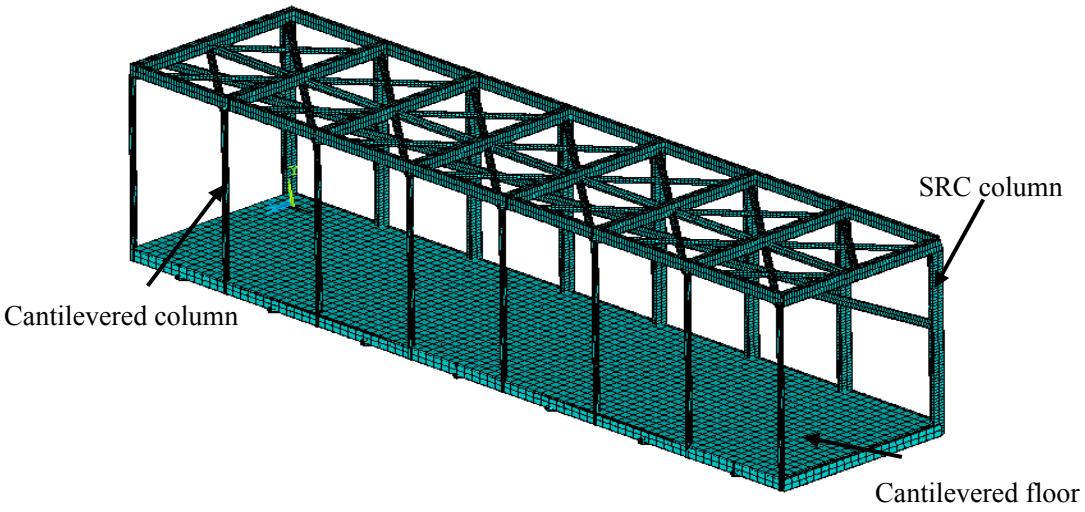

(a)

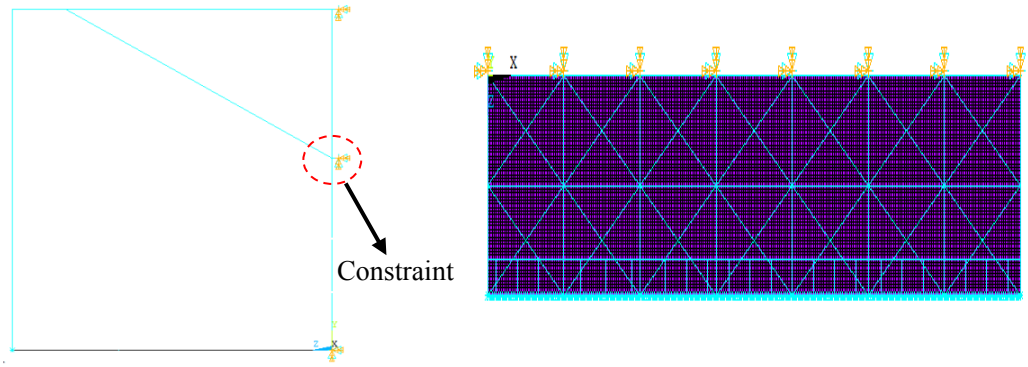

Fig. 7. FE Model: (a) size shape of isometric view (b) Right view(c) top view

3.3.2 Equivalent approaches for glass curtain wall in numerical analysis

The effect of glass curtain wall structural system on structural analysis was also simplified. Currently, there are two popular approaches for this considering the interaction between glass curtain wall and integral structure: one is simplified as equivalent mass distributed along its position; the other is as the equivalent vertical stiffness contributing to the structure [4]. The results are shown in Table 2.

Compared the mode results between field tests and FE analysis, the existing equivalent approaches for the glass curtain wall cannot agree well with the experiment. The mode1 frequency of the floor using the equivalent approach I for the glass curtain wall was 2.80 Hz, and the error was 16.67% compared with the experimental value of 3.36 Hz. While for the approach Π, the value was 2.82 Hz with an error of 16.07%. Moreover, the following frequencies were also underestimated with large difference and the mode shapes differed greatly compared with the experiment. The deviation occurred in the approach I could be explained as the contribution of glass curtain wall to floor stiffness was neglected even though the weight of glass curtain wall was taken into account in the current practice. For the approach II, both the contributions of glass curtain wall weight and stiffness were considered; however, only the vertical stiffness was equivalent by the axial vertical spring, neglecting the weak constraint effect of glass curtain wall. Based on the results, mode and vibration responses, a weak constraint of glass curtain effect should be proposed and considered, and then the FE model was revised.

Table 2

Comparison for the structural frequencies between the experimental results and the simplified approaches for the glass curtain wall

Mode	approach I	approach Π	Experimental	Error between approach I and experimental / %	Error between approach Π and experimental/ %
1	2.80	2.82	3.36	16.67	16.07
2	3.02	3.04	4.13	26.88	26.39
3	3.54	3.57	5.23	32.31	31.74
4	4.29	4.34	6.63	35.29	34.54
5	5.38	5.46	7.38	27.10	26.02
6	6.63	6.75	8.08	17.95	16.46

3.4 Updated FE model based on the weak constraint effect

To ensure the accuracy of numerical analysis, the model should be updated according to the

experimental results. Zhu et al. [35] realized the adjustability of floor frequency and then achieved different degrees of vibration reduction by selecting semi-rigid supports with different stiffness ratios. Here, the spring damper, COMBIN14, was used to simulate the slip between beams and columns. Secondly, according to the weak constraint effect of glass curtain wall, the equivalent stiffness approach was employed to study the effect of the glass curtain wall on the stiffness of truss columns and then the glass curtain wall was considered in the modal calculation of floor vibration.

3.4.1 Weak constraint effect

Glass curtain wall, its skeleton and supported row-column constitute a space system, as shown in Fig. 8(a). Compared with the original single row-column, the system has a constraint effect: the in-plane lateral stiffness of the system increases by multiples of geometric series. Diamond or rectangular skeletons are generally adopted in the glass curtain wall, and the out-of-plane lateral stiffness of the wall also increases with skeleton constraints through connectors. Moreover, glass curtain walls are generally connected with row-columns through the skeleton, as shown in Fig. 8(b); the restraint of the floor is also reinforced through row-columns, which is different from the commonly constructed wall. Because of weak linkages between elements, the lateral stiffness of the system is smaller than that of the bare wall of the same shape. The glass curtain wall restraint on the floor structure above can be called as the weak constraint effect.

(a)

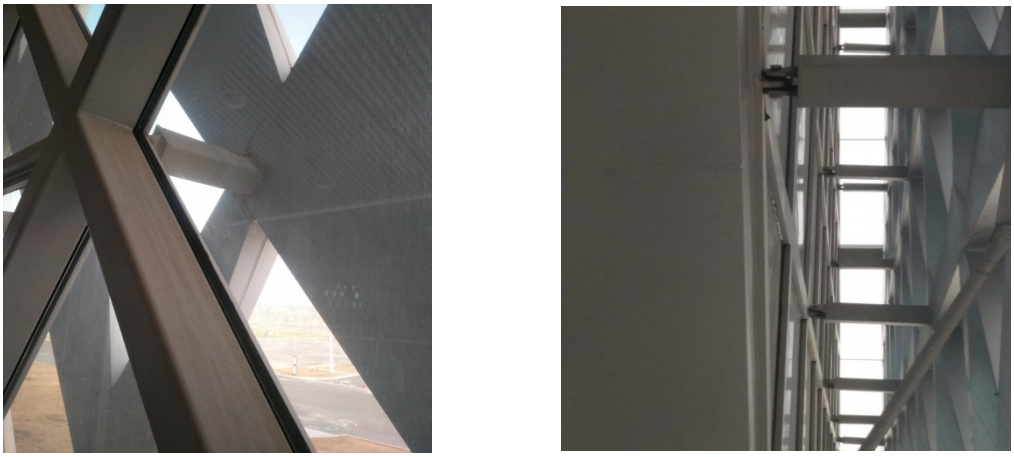

(b)

Fig. 8. Glass curtain wall of the on-site: (a) elevation of glass curtain wall (b) connections between glass curtain wall skeletons.

Because of the glass curtain wall, the whole stiffness of the cantilevered column significantly increases. For example, the lattice column's stiffness is much larger than that of several single columns. Therefore, the weak constraint effect significantly improves the whole inertia moment of the cantilevered column. According to the weak constraint effect of glass curtain, an equivalent approach was adopted to consider the role of the glass curtain wall in the FE. The equivalent mass was simulated by the MASS21 element, and the contribution of the glass curtain wall to the stiffness of the floor was achieved by increasing the stiffness of the cantilevered column with equal strength. The equivalent principle in ANSYS was to increase the elastic modulus of the cantilevered column by multiples of different series to achieve the weak constraint stiffness of glass curtain wall. The specific value was determined by the comparison with experimental results.

3.4.2 Mode comparison between the updated FE model and field tests

Referring to the experimental results of structural vibration frequencies and modes, the stiffness of the cantilevered column was increased by multiple series based on the weak constraint effect. In order to quickly estimate the equivalent cantilevered column stiffness of the weak constraint effect of the glass curtain wall, it is assumed that the glass curtain wall and cantilevered column are of the same material. Therefore, the ratio of out-of-plane stiffness is equivalent to the ratio of section inertia moment, in this case, the number of cantilevered columns is 8, and the section is 300 *mm* × 300 *mm*, the thickness of glass curtain wall is 200 *mm*, and the distance between the glass curtain wall and cantilevered column is 400 *mm*. The stiffness of the cantilevered column calculated with the knowledge of mechanics of materials is approximately 700 series of the real wall equivalent. In the real case, the moment of inertia of the equivalent cantilevered column is approximately 1:2 of the solid wall, about 350 series to 700 of the solid wall. Consequently, when the stiffness of the cantilevered column was increased by 500 series, the numerical results of vibration modes agreed well with the experimental results, as shown in Fig. 9. The vertical vibration frequencies obtained from the updated FE were 3.37, 4.06, 5.15, 6.35, 7.46, and 8.31 Hz, respectively (see Table 3). Here, the modal characteristics of the floor and cantilevered columns were extracted separately.

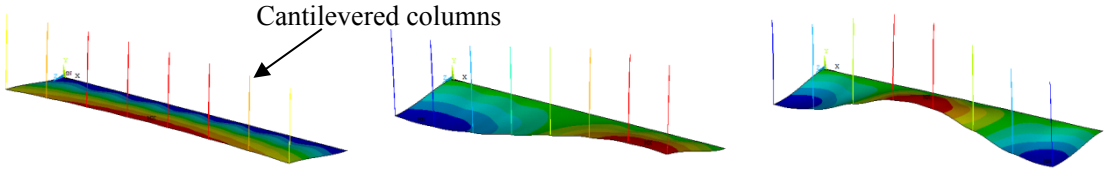

(a1) FE Mode 1：$f_1 = 3.37$ Hz (b1) FE Mode 2：$f_2 = 4.06$ Hz (c1) FE Mode 3：$f_3 = 5.15$ Hz

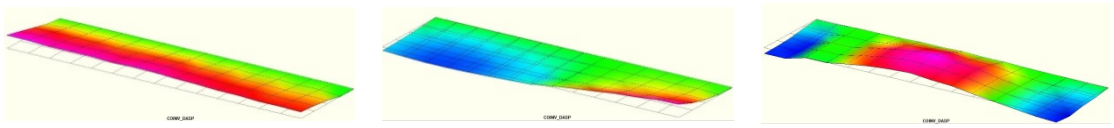

(a2) SSI Mode 1：$f_1 = 3.36$ Hz (b2) SSI Mode 2：$f_2 = 4.13$ Hz (c2) SSI Mode 3：$f_3 = 5.23$ Hz

(a) comparison of mode 1 (b) comparison of mode 2 (c) comparison of mode 3

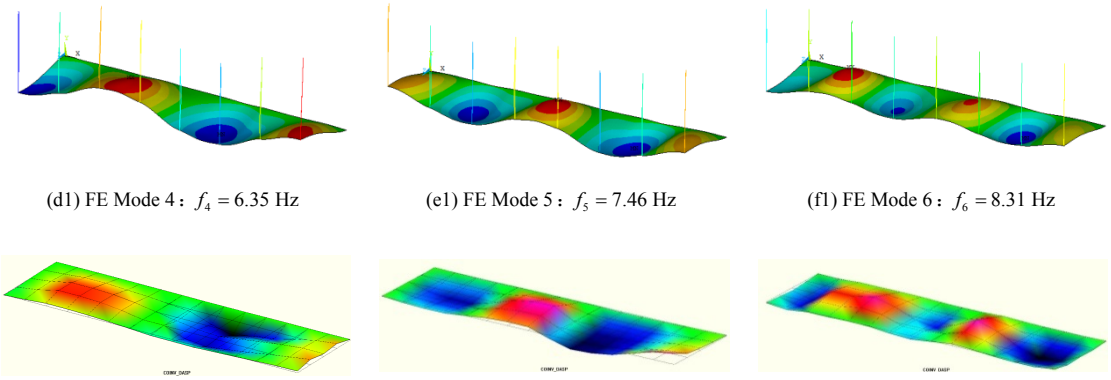

(d1) FE Mode 4： $f_4 = 6.35$ Hz (e1) FE Mode 5： $f_5 = 7.46$ Hz (f1) FE Mode 6： $f_6 = 8.31$ Hz

(d2) SSI Mode 4： $f_4 = 6.63$ Hz (e2) SSI Mode 5： $f_5 = 7.38$ Hz (f2) SSI Mode 6： $f_6 = 8.08$ Hz

(d) comparison of mode 4 (e) comparison of mode 5 (f) comparison of mode 6

Fig. 9. Comparison between experimental and numerical (updated model) mode shapes.

The results showed that the vibration frequency between numerical and experimental results agreed well, as shown in Table 3. The error of each frequency was less than 5% and average errors were 1.93%, which was an excellent satisfied result after considering the weak constraint effect. Therefore, it is reasonable to increase the stiffness of the cantilevered column to represent the weak constraint effect, and then the effect of weak constraint of glass curtain has also been demonstrated.

Table 3

Comparison between experimental and numerical (updated model) natural frequencies

Mode	Numerical（Hz）	Experimental （Hz）	Relative error / %
1	3.37	3.36	0.30
2	4.06	4.13	1.69
3	5.15	5.23	1.53
4	6.35	6.63	4.22
5	7.46	7.38	1.07
6	8.31	8.08	2.77
Average error/ %		1.93	

4. Human-induced vibration responses analysis

4.1 Experimental preparation for human-induced vibration

In order to obtain the maximum acceleration response in field tests, a total of nine test points were selected for placing accelerometers on floor where the weakest location of mode shape, as shown in Fig. 10. Two representative routes were selected: Route 1 was along the longitudinal direction of the floor, and Route 2 was along the transverse direction of the floor, similar to the FE walking route in Fig. 14. Then, the number of testers is determined, referring to the walking density of the crowd, and selected 0.385 pedestrians/m^2 similarly a quasi-free state as the design factor according to the *American Road Traffic Capacity Manual HCM2000* and the practical function of the cantilevered floor. Finally, we determined the maximum number of testers as 72 people (72 synchronized walking is equivalent to 360 people quasi freely walking, N~0.2n [36]),

as shown in Fig. 11, and also conducted single, 20, and 40 pedestrian synchronized walking. The corresponding number of synchronized crowds under different walking densities is shown in Table 4.

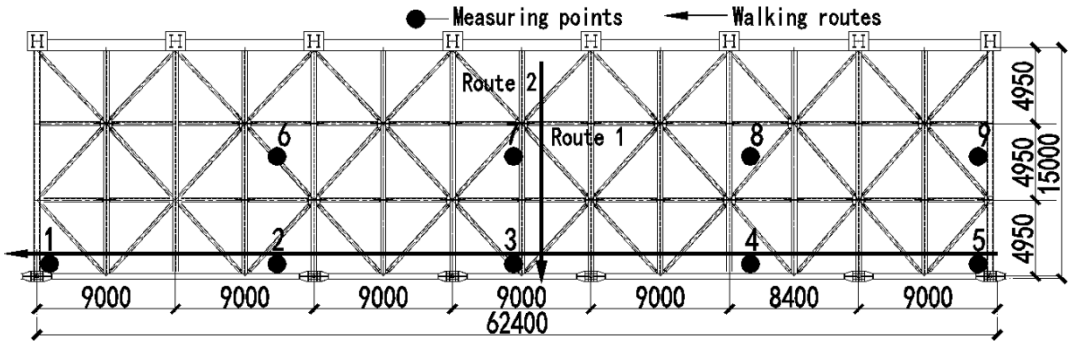

Fig. 10. Location of the accelerometers and two walking routes on the field test.

4.2 Field test results for human-induced vibration analysis

After designing the test points and walking route, based on the existing walking frequency range and structure frequency, 1.68 Hz (half of the first vertical frequency) resonance frequency was determined as walking frequency, The configurations included single people and group people (body weight range: 45–90 kg, mean value: 66 kg) walking in same pace rate under the control of a metronome. Due to the limited space, only partial excitation conditions of Route 2 were selected for discussion. Figs. 12–13 show the human-induced acceleration time history response of the floor.

Table 4

Pedestrian traffic classes and density.

Description	Person per unit area (pedestrians/m^2)	Number of Walkers (pedestrians)	Synchronized Number (pedestrians)
Walking freely	0.106	100	20
	0.203	200	40
Quasi freely	0.385	360	72

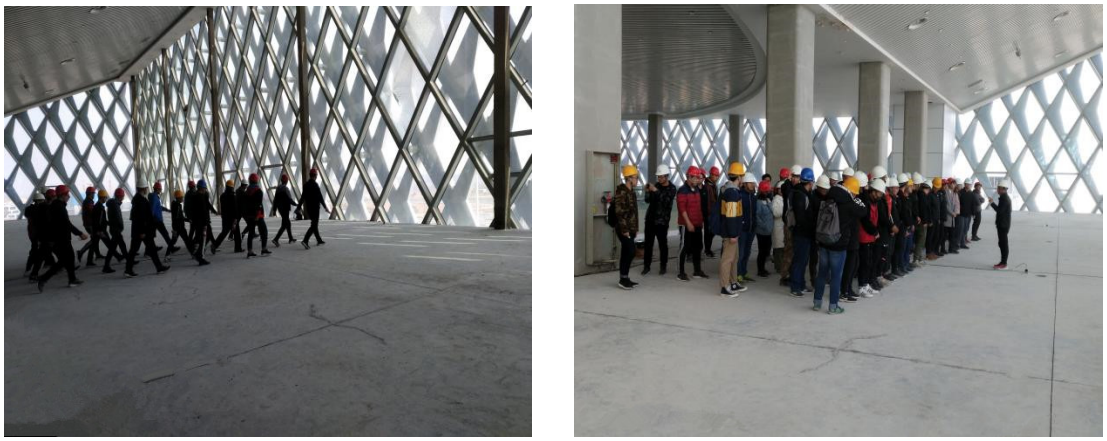

(a) (b)

Fig. 11. Field test: (a) 20 pedestrians walking (b) 72 pedestrians walking.

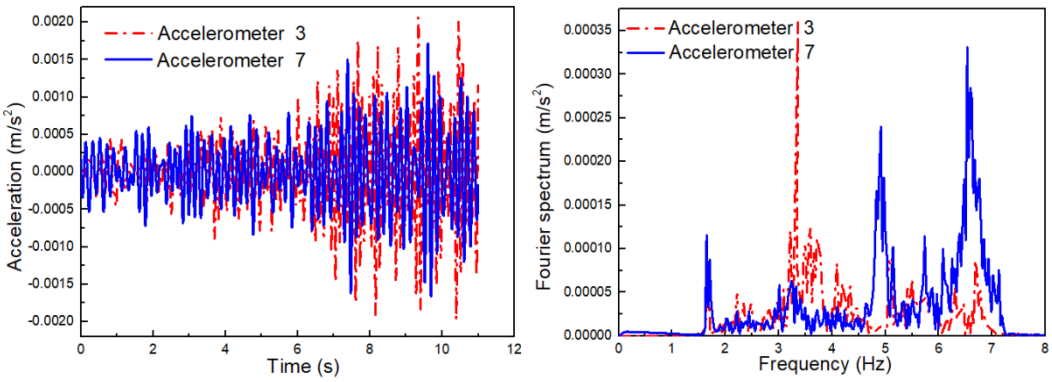

(a) (b)

Fig. 12. Acceleration time history and FFT spectrum of different measuring points for walking of a single pedestrian: (a) Acceleration time history (b) FFT spectrum.

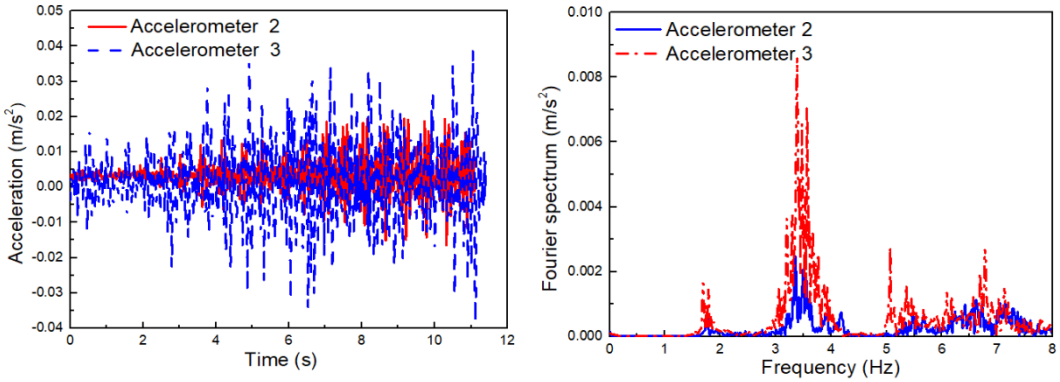

(a) (b)

Fig. 13. Acceleration time history and FFT spectrum of different measuring points for walking of 20 pedestrians: (a) Acceleration time history (b) FFT spectrum.

By comparing the acceleration response and FFT spectrum of selected points from Figs. 12–13, it can be found that a significant sub-harmonics frequency component appears in the measured response. Furthermore, the FFT spectrum of test point 2 and 3 is mainly 3.4 Hz since it is located near the first vertical frequency, while the high frequency is the main frequency of test point 7 in the middle of the span. From the time domain curve, the acceleration response of the cantilevered floor is different from that of the ordinary floor, which is generally large in the middle and small on both sides because of the constraints condition. However, the response in the cantilevered floor tends to increase continually along the cantilevered direction. The acceleration response is up to the maximum at the point of the first vertical frequency peak. The results of all measured points were concluded in Table 5.

Table 5

Peak accelerations in different loading conditions.

Number of pedestrians	Acceleration response value of each channel (m/s^2)								
	#1	#2	#3	#4	#5	#6	#7	#8	#9
1	0.001412	0.00079	0.00206	0.00063	0.00086	0.0005	0.0017	0.0004	0.0005
20	0.0149	0.018	0.04	0.011	0.016	0.022	0.038	0.02	0.025
40	0.0207	0.02	0.083	0.032	0.027	0.048	0.08	0.058	0.059

It is obvious that the peak acceleration of the floor under pedestrians' load is larger than that under a single pedestrian. Under synchronized walking excitation, the mean accelerations of single pedestrian, 20 pedestrians, and 40 along Route 2 were 0.000983 m/s^2, 0.0228 m/s^2, and 0.0475 m/s^2, respectively. Among them, measuring #3 was the largest displacement point of the mode 1 and thus was the main point discussed in this paper. The peak acceleration of #3 for a single pedestrian was 0.00206 m/s^2, 20 pedestrians increasing to 0.04 m/s^2; thus, the response increased about 20 times. When the number of pedestrians increased to 40, the peak acceleration was 0.083 m/s^2.

The restriction of maximum acceleration of structure has been limited referring to Murray Specifications [34] for the peak acceleration values of operating rooms, offices, residential buildings, shopping malls, and restaurants. According to the function of the cantilevered floor (lounge), the vertical acceleration limit of the floor is 0.15 m/s^2. It can be seen that under the excitation of synchronous walking, the peak acceleration of the floor does not exceed the serviceability assessment standard.

4.3 Numerical vibration response without HSI

Since the pedestrian load is composed of main harmonics and sub-harmonics, it is necessary to define the amplitude of each them. It is a bit complicated as the existence of energy spreading around the main harmonics and sub-harmonics, it can be equivalent. For each of them, a sinusoidal load can be defined in such a way that its power is equal to the power of the analyzed (sub) harmonics. A coefficient can be obtained from the amplitude of this sinusoid divided by the subject's weight, which is commonly accepted for characterization of each load (sub) harmonics. This value is called the dynamic loading factor (DLF) [18].

For the i^{th} harmonic, occurring at frequency if_p, the main harmonics could be obtained from the Eq. (1):

$$F_i(t) = \sum_{i=1}^{3} \alpha_i \sin(2\pi i f_p - \varphi_i) \tag{1}$$

While for the i^{th} sub-harmonics, it would be

$$F_i^s(t) = \sum_{i=1}^{3} \beta_i \sin(2\pi i f_p^s - \varphi_i^s) \tag{2}$$

Here, f_p is the walking pacing frequency (Hz), the power for each sub-harmonics f_p^s was calculated in the frequency range, it would be more appropriate to call the harmonic appearing at a frequency of $(i-0.5)f_p$. φ_i and φ_i^s is the phase angle, which is based on a uniform distribution of phases in the interval $[-\pi, +\pi]$; i is the sub-harmonics considered (i = 1,2,3…), and α_i is the dynamic loading factor, the DLFs for sub-harmonics β_i can be considered as independent from DLF1(α_1), $\beta_1 = 0.026\alpha_1 + 0.031$, $\beta_2 = 0.074\alpha_1 + 0.001$, $\beta_3 = 0.012\alpha_1 + 0.001$. Finally, the total force can be obtained by Eq. (3):

$$F(t)=\sum_{i=1}^{3}F_i(t)+\sum_{i=1}^{3}F_i^s(t) \tag{3}$$

In the numerical analysis, only the vertical pedestrian load is loaded into the structural FE nodes according to the time sequence, where the HSI is not considered when simulating a single pedestrian load and multiple pedestrians load. As shown above, the first vertical frequency of the modified FE model was 3.37 Hz. Thus the walk pacing frequency of 3.37/2 = 1.68 Hz was determined in the model and with a step length of 0.75 m. To make a comparison with experimental results, two routes were used: Route 1 was the longitudinal direction of the floor, and Route 2 was the lateral direction, as shown in Fig. 14. Each load route was set to pass through the peak point of the first mode. Therefore, the maximum acceleration response in the numerical analysis of the node number 12554 which also have the maximum displacement amplitude in the first vibration mode was compared with the response of #3 (in experimentally measured points) , which was along Route 2 under different excitations, as shown in Figs. 15–17. The peak acceleration response of the floor at the same position is listed in Table 6.

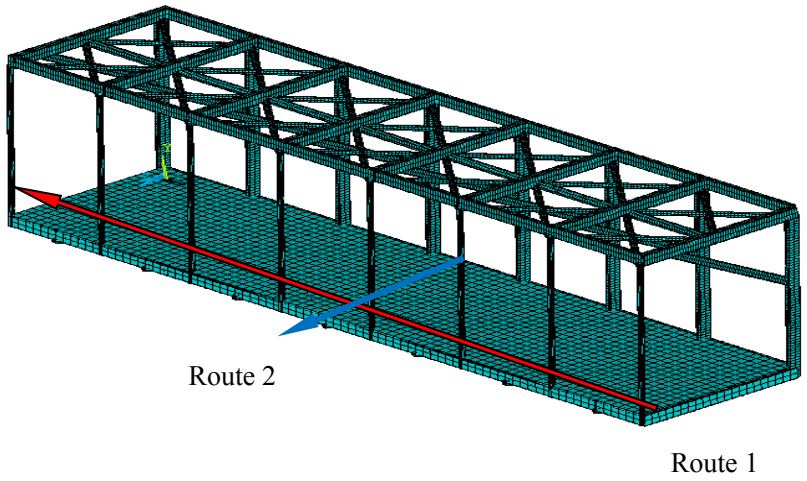

Fig. 14. Two walking routes on the test floor.

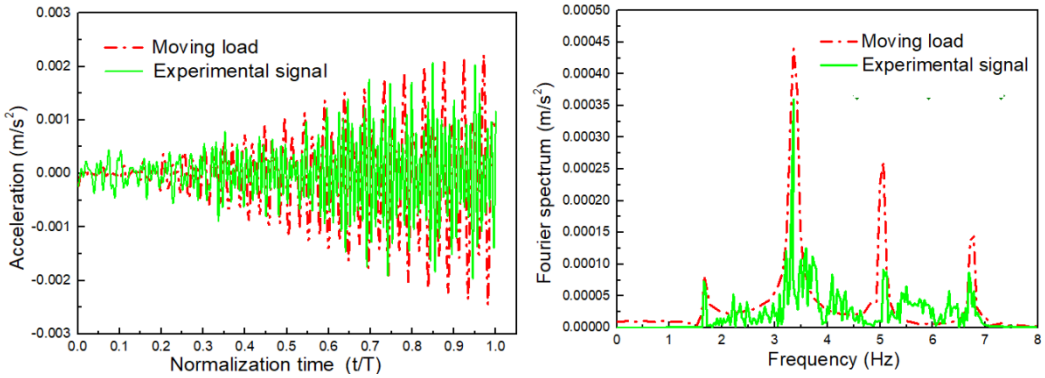

(a) (b)

Fig. 15. Comparison of acceleration time history and FFT spectrum curve of walking of a single pedestrian: (a) Acceleration time history (b) FFT spectrum.

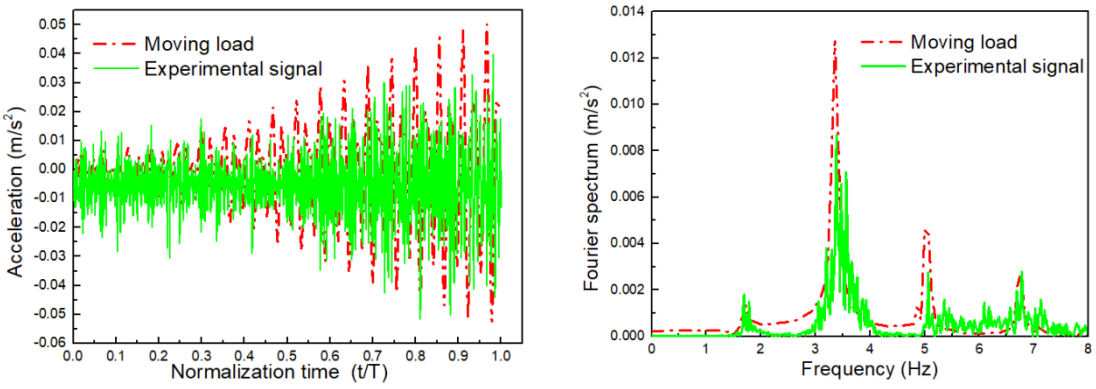

(a) (b)

Fig. 16. Comparison of acceleration time history and FFT spectrum curve of walking of 20 pedestrians: (a) Acceleration time history (b) FFT spectrum.

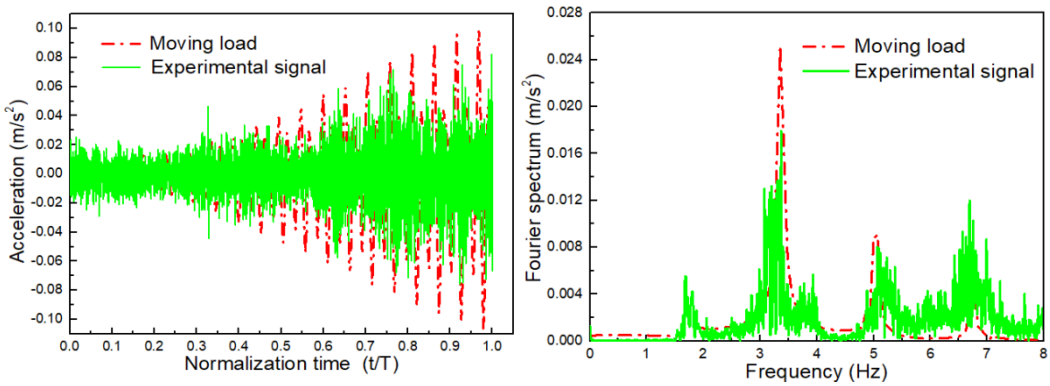

(a) (b)

Fig. 17. Comparison of acceleration time history and FFT spectrum curve of walking of 40 pedestrians: (a) Acceleration time history (b) FFT spectrum.

Table 6

Comparison between experimental and numerical of structural responses.

Number of walking pedestrians	Vertical acceleration (m/s²)		
	Moving load	Experimental signal	Error (%)
Single rhythm walking	0.00222	0.00206	7.21
20 people walking in rhythm	0.0504	0.040	20.63
40 people walking in rhythm	0.1003	0.083	12.05
72 people walking in rhythm	0.1233	0.102	17.27

It can be seen from Figs. 15–17 that when the load model with multi-harmonic and sub-harmonics components is constructed by referring to Živanović [18] in the pedestrian load model, the spectrum of the FE is closer to the measured, but the acceleration time history without considering the human structure interaction are larger. Table 6 shows that the acceleration response induced by a single pedestrian was close for different conditions of considering whether HSI is considered or not. However, if HSI is not considered, the peak acceleration of 20

pedestrians' load was 0.0504 m/s^2, which was 20.63% higher than the experimental result 0.04 m/s^2. Similarly, the peak acceleration of 40 pedestrians' load without considering the HSI was 0.1003 m/s^2, which is 17.25% higher than the experimental result of 0.083 m/s^2, as shown in Table 6. Therefore, it can be concluded that only using only a Fourier series load model to represent the pedestrian load leads to a large error compared with the experimental test or the real response in the structure.

4.4. Numerical vibration response with HSI

4.4.1 Biodynamic model of pedestrian for HSI

In order to consider the coupling human-structure vibration, a single-degree-of-freedom (SDOF) biodynamic model was employed in this section, as shown in Fig. 18. Among them, m_p, k_p, and c_p represent the mass, stiffness, and damping of the human body. F_t represents the pedestrian load, u_p represents the pedestrian vertical displacement, and u represents the vertical displacement of the cantilevered floor.

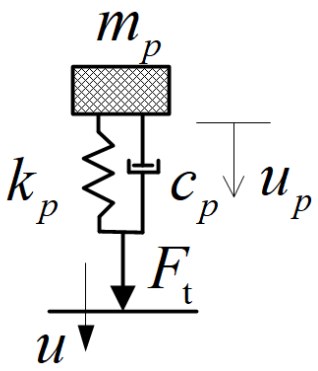

Fig. 18. Single-degree-of-freedom biodynamic model.

The regression expression of human parameters can be expressed as the function of body weight M and pedestrian walking frequency, as shown in Eqs. (4–6) [25].

$$m_p = 97.082 + 0.275M - 37.518f_p \tag{4}$$

$$c_p = 29.041m_p^{0.883} \tag{5}$$

$$k_p = 30351.744 - 50.261c_p + 0.035c_p^2 \tag{6}$$

where M is the pedestrian weight and f_p is the walking frequency.

4.4.2 Comparison between experimental and numerical vibration response with and without HSI

When considering the interaction between humans and structure, the established SDOF biodynamic model was used to human load combined with Fourier series load model and then applied to the FE model. The movable pedestrian load was realized by the deactivation elements when walking along the routes in the numerical analysis. Figs. 19–21 show the comparison of acceleration time history curves and FFT spectrum with versus without considering HSI. The peak acceleration can be seen in Table 7.

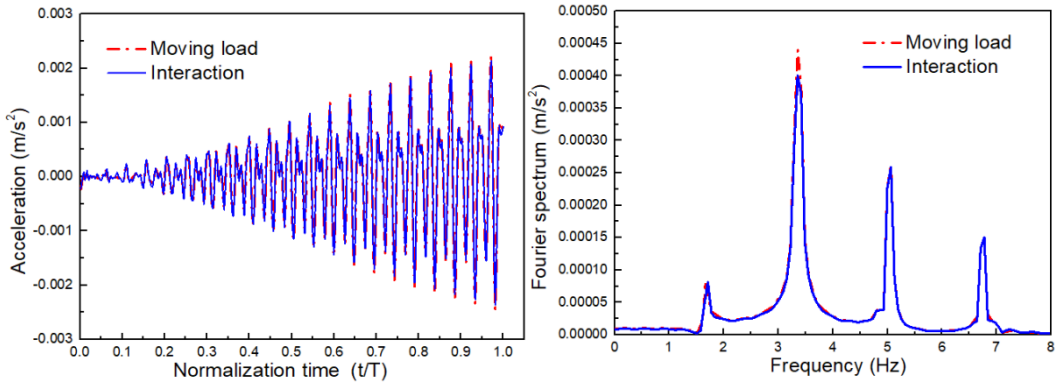

(a) (b)

Fig. 19. Comparison of acceleration time history and FFT spectrum curve of walking of a single pedestrian: (a) Acceleration time history (b) FFT spectrum.

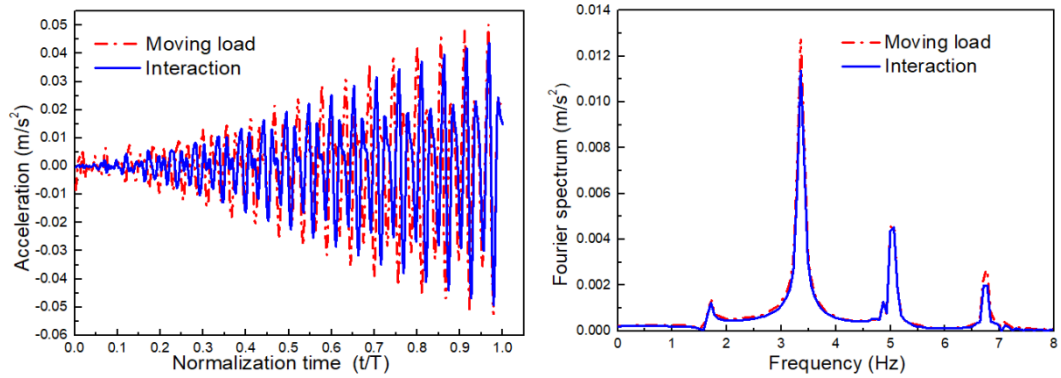

(a) (b)

Fig. 20. Comparison of acceleration time history and FFT spectrum curve of walking of 20 pedestrians: (a) Acceleration time history (b) FFT spectrum.

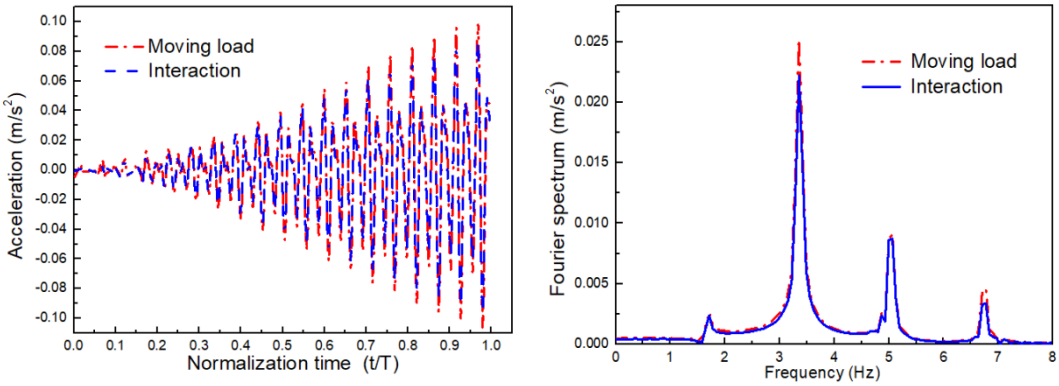

(a) (b)

Fig. 21. Comparison of acceleration time history and FFT spectrum curve of walking of 40 pedestrians: (a) Acceleration time history (b) FFT spectrum.

Table 7

Maximum recorded accelerations due to walking.

Number of walking pedestrians	Vertical acceleration (m/s^2)		
	Moving load	Interaction	Experimental signal
Single rhythm walking	0.00222	0.00213	0.00206
20 people walking in rhythm	0.0504	0.0437	0.040
40 people walking in rhythm	0.1003	0.0865	0.083
72 people walking in rhythm	0.1233	0.1083	0.102

The peak acceleration of the floor under different locations was compared. The peak acceleration of the floor decreased when the HSI was considered. Among them, when 20 pedestrians walked synchronously, the peak value of the HSI acceleration was 0.0437 m/s^2, which is 13.29% lower than that without considering the HSI acceleration (0.0504 m/s^2). The peak acceleration of the synchronous walking of 40 pedestrians was 0.0865 m/s^2, which is 13.76% lower than that without considering the interaction (0.1003 m/s^2). Considering the HSI under the pedestrians' load, the effect on the vibration response of the structure is apparent, whereby the results are consistent with the literature [6, 14]: if the interaction between pedestrian and structure is neglected, the dynamic response of the structure will be overestimated. Therefore, the establishment of the human biomechanical model is of great significance to further explore the pedestrian-structure dynamic interaction.

Finally, the comparison of the Fourier series loading model and the biomechanical model of the floor simulated by the FE approach is shown in Figs. 22–24, respectively. The peak acceleration of the floor at the same location in three cases is listed in Table 8.

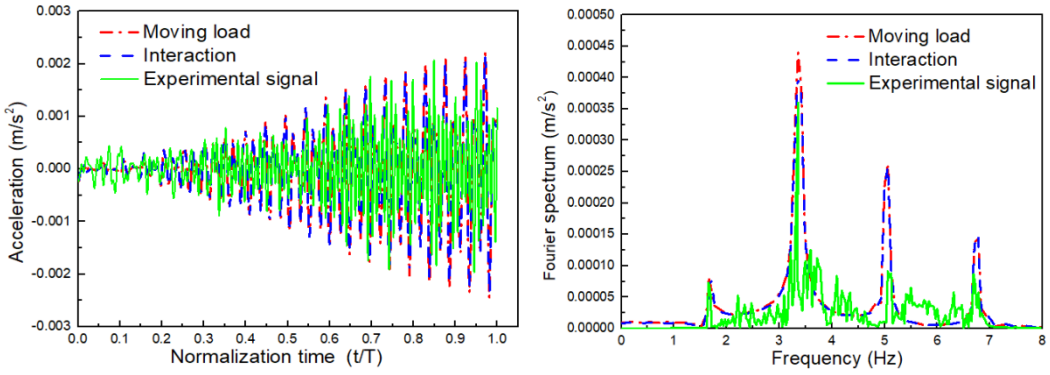

(a) (b)

Fig. 22. Comparison of acceleration time history and FFT spectrum curve of walking of a single pedestrian: (a) Acceleration time history (b) FFT spectrum.

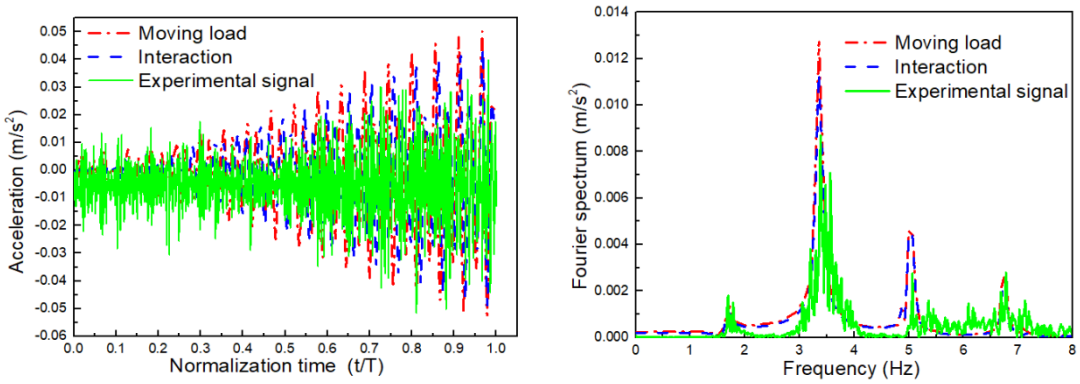

(a) (b)

Fig. 23. Comparison of acceleration time history and FFT spectrum curve of walking of 20 pedestrians: (a) Acceleration time history (b) FFT spectrum.

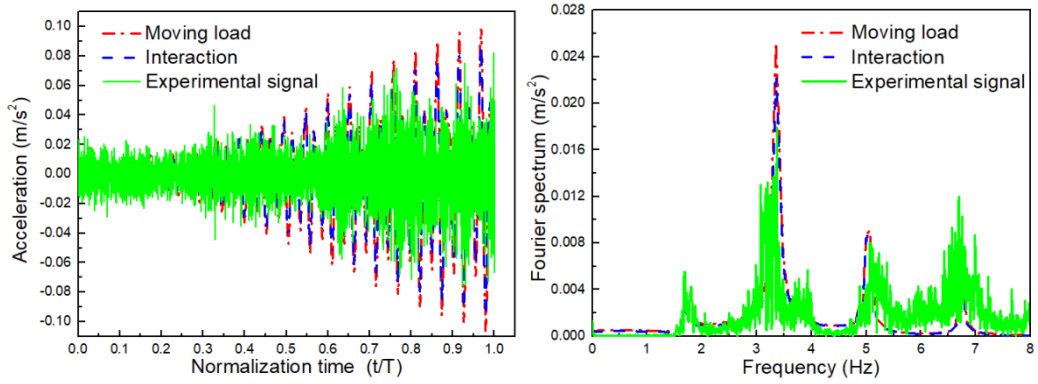

(a) (b)

Fig. 24. Comparison of acceleration time history and FFT spectrum curve of walking of 40 pedestrians: (a) Acceleration time history (b) FFT spectrum.

Table 8

Comparison between experimental and numerical results of human-induced vibration.

Number of walking pedestrians	Vertical acceleration (m/s²)			
	Moving load	Interaction	Experimental	Error between interaction value and experimental
1	0.00222	0.00213	0.00206	3.28%
20	0.0504	0.0437	0.04	8.47%
40	0.1003	0.0865	0.083	4.05%
72	0.1233	0.1083	0.102	5.82%

Table 8 shows that the peak acceleration of walking of 20 pedestrians considering the HSI was 0.0437 m/s², which gives an 8.47% deviation compared with the measured peak acceleration of 0.04 m/s². The peak acceleration of walking of 40 pedestrians considering the HSI was 0.0865 m/s², giving 4.05% error compared with the measured peak acceleration of 0.083 m/s².When 40 pedestrians walked, the peak acceleration of considering HSI was 0.0865 m/s², giving a 4.05% error compared with the measured peak acceleration of 0.083 m/s².

Therefore, the acceleration response of human-induced vibration calculated by the FE approach did not agree well with the measured results because the load of the crowd was simulated with a Fourier series only. The biomechanical model equivalent to the crowd load with main harmonics and sub-harmonics components is closer to the experimental results. The reliability of the biomechanical model is further confirmed. The results further indicate that the human-structure coupling vibration is essential for serviceability assessment.

5. Discussion

In this paper, the weak constraint effect was proposed for the curtained wall acting as a non-structural component. Then, the FE model was updated by considering the contribution of the curtained wall to floor stiffness. The updated FE vibration mode was in excellent agreement with the experimental results. The weak constraint effect of glass curtain wall was proposed based on the existing specification [34]. We presented the research results on increasing the frequency and mode of the floor by providing stiffness contribution for non-structural members. However, a large number of theoretical and experimental studies are still needed on the weak constraint effect of glass curtain and its quantitative formula of stiffness.

When simulating the HSI, the structural damping ratio was selected according to the damping ratio of the floor under ambient excitation and calculated according to the same damping ratio. Existing studies show that the damping ratio of the structure is related to the amplitude of the floor, and the damping ratios of the floor under the action of a person will be different as opposed to that of multiple pedestrians [37]. Therefore, the structural damping ratio needs to be further studied and analyzed to obtain the damping ratio suitable for the FE modeling of the floor.

The gait cycle will change from 3% to 4% in the course of walking. Even under the control of the metronome, the gait cycle will change while the change range will be rather small [38]. For the walking frequency of the crowd, this paper simplifies the loading according to the same step frequency. However, more accurate FE models should take frequency variations into account.

For single person walking, there is little difference between the acceleration with and without HSI, only 4.05%, while for crowd, HSI cannot be ignored, such as 20 and 40 pedestrians, the difference is 13.29% and 13.76%, respectively. However, The SMD model we proposed in this paper, needs to be further verification and improvement by referring to the existing narrow-band model Živanović [18], the inter-subject variability, such as walking frequencies, force amplitudes, and step lengths need to be further studied, so as to for better agreement between FEM and experimental.

6. Conclusions

In this paper, the experimental investigation and numerical analysis on structural vibration mode and response were conducted. The FE model for the whole structure was updated comparing with the field test based on the effect of weak constraint of glass curtain. The human-induced vibration was systematically analyzed and compared with field test and clarified the significance of HSI. The structural serviceability was evaluated experimentally and numerically, which also provide reference for the human-induced vibration analysis. Several important conclusions are summarized as follows.

(1) Comparing with the field test for structural vibration mode, the FE model was updated by addressing the effects of non-structural components, i.e. the glass curtain wall and showed that it had an effect on the structural vibration characteristics. Neglecting the weak constraint effect of

glass curtained wall for the mode and vibration serviceability analysis may lead to conservative design results.

(2) Comparing the numerical results of human-induced acceleration response with and without consideration of the HSI, the latter case overestimated the structural response. For example, when 20, 40, and 72 pedestrians walked synchronously, the peak accelerations considering the HSI were 13.29%, 13.76%, and 12.16% less than that without considering the interaction, respectively. Thus, considering the HSI led to different result for acceleration response. .

(3) Comparing the structural responses under the Fourier series load and SMD model, with the field test results respectively, it was demonstrated that FE analysis considering the HSI and sub-harmonics component was in good agreement with the experimental results. For example, the peak acceleration of walking of 20 pedestrians without considering the HSI was 0.0504 m/s^2, which is 20.63% higher than the measured peak acceleration (0.04 m/s^2), while the peak acceleration of walking of 20 pedestrians considering the HSI was 0.0437 m/s^2, which is 8.47% higher than the measured peak acceleration. Therefore, in order to obtain a more accurate human-induced vibration serviceability evolution in FE analysis, the HSI and, sub-harmonics components should be taken account.

Acknowledgments

This work was supported by the National Natural Science Foundation of China (No. 51668042, 51868046, and 51508257) and the China Scholarship Council (No. 201808620022).

References

[1] Zheng X, Brownjohn, JMW. Modeling and simulation of human-floor system under vertical vibration //Smart Structures and Materials 2001: Smart Structures and Integrated Systems. International Society for Optics and Photonics, 2001, 4327: 513-520.

[2] Pavic A, Reynolds P. Vibration serviceability of long-span concrete building floors. Part 1: Review of background information. Shock and Vibration Digest, 2002, 34(3): 191-211.

[3] Drygala I J, Dulinska J M. A theoretical and experimental evaluation of the modal properties of a cable-stayed footbridge. Procedia Engineering, 2017, 199: 2937-2942.

[4] Devin, A, Fanning P J, Pavic A. Modelling effect of non-structural partitions on floor modal properties. Engineering Structures，2015，91：58-69.

[5] Setareh M.Vibration Serviceability of a Building Floor Structure. I: Dynamic Testing and Computer Modeling. Journal of Performance of Constructed Facilities，2010，24(6)：497-507.

[6] Salyards K A, Noss N C. Experimental evaluation of the influence of human-structure interaction for vibration serviceability. Journal of Performance of Constructed Facilities, 2013, 28(3): 458-465.

[7] Petrovic S, Pavic A. Effects of non-structural partitions on vibration performance of floor structures: A Literature Review//Int. Conf. Struct. Dyn.(EURODYN 2011), Leuven, Belgium. 2011.

[8] Miskovic Z, Pavic A, Reynolds P. Effects of full-height nonstructural partitions on modal properties of two nominally identical building floors. Canadian journal of civil engineering, 2009, 36(7): 1121-1132.

[9] Jarnerö K., Brandt A., Olsson A. Vibration properties of a timber floor assessed in laboratory and during construction. Engineering structures, 2015, 82: 44-54.

[10] Rijal R, Samali B, Shrestha R, et al. Experimental and analytical study on dynamic performance of timber floor modules (timber beams). Construction and Building Materials, 2016, 122: 391-

399.
[11] Chen J, Yan S, Zhang M. Vibration performance assessment of a long-span concrete floor using field measurements over a five-year period. Advances in Structural Engineering, 2014, 17(8): 1145-1158.
[12] Fanning P J, Devin,A. Vibration Transmission Through Non-Structural Partitions Between Building Floor Levels//Dynamics of Civil Structures, Volume 2. Springer, Cham, 2016: 297-302.
[13] Pavic A, Widjaja T, Reynolds P. The use of modal testing and FE model updating to investigate vibration transmission between two nominally identical building floors//Proc., Int. Conf. on Structural Dynamics Modeling-Test, Analysis, Correlation and Validation. Lisbon, Portugal: Instituto Superior Tecnico, 2002: 347-355.
[14] Ellis B R, Ji T, BRE. Human-structure interaction in vertical vibrations. Proceedings of the Institution of Civil Engineers-Structures and Buildings, 1997, 122(1): 1-9.
[15] Zhu Q K, Hui X L, Nan N N, et al. Study on the Vertical Dynamic Coupled Effects of the Crowd-structure System based on the Social Force Model. KSCE Journal of Civil Engineering. 2019,23(5):2243-2253
[16] Feldmann M, Heinemeyer C, Lukic M. Design of Footbridges. Guideline. Human Induced Vibrations of Steel Structure (Hivoss). 2008.
[17] Steel B S I. concrete and composite bridges. Specification for loads, BS 5400: Part 2. British Standard Institution, 1978.
[18] Živanović S, Pavić A, Reynolds P. Probability-based prediction of multi-mode vibration response to walking excitation. Engineering Structures, 2007, 29(6): 942-954.
[19] Brownjohn J M W, Pavic A, Omenzetter P. A spectral density approach for modelling co ntinuous vertical forces on pedestrian structures due to walking. Canadian Journal of Civil Engineering, 2004, 31(1): 65-77.
[20] Živanović S, Pavic A, ReynoldsP. Human–structure dynamic interaction in footbridges//Pro ceedings of the Institution of Civil Engineers-Bridge Engineering. Thomas Telford Ltd, 20 05, 158(4):165-177.
[21] Sachse R, Pavic A, Reynolds P. The influence of a group of humans on modal properties of a structure//Proceedings of the fourth international conference on structural dynamics. 2002, 2: 1241-1246.
[22] Barker C, Mackenzie D. Design methodology for pedestrian induced footbridge vibrations. Proceedings of footbridge, 2008.
[23] Lenzen K H. Vibration of steel joist-concrete slab floors. AISC. Eng. Jour., 1966, 3: 133-136.
[24] Kim S H, Cho K I, Choi M S, et al. Development of human body model for the dynamic analysis of footbridges under pedestrian induced excitation. Steel Structures, 2008, 8: 333—345.
[25] Silva F T, Pimentel R L. Biodynamic walking model for vibration serviceability of footbridges in vertical direction//Proceeding of the 8th International Conference on Structural Dynamics (Eurodyn'11). 2011: 1090-1096.
[26] Da Silva F T, Brito H M B F, Pimentel R L. Modeling of crowd load in vertical direction using biodynamic model for pedestrians crossing footbridges. Canadian Journal of Civil Engineering, 2013, 40(12): 1196-1204.
[27] Dang H V, Zivanovic S. Modelling pedestrian interaction with perceptibly vibrating footbri dges．FEM Transactions，2013,41(4):271-278
[28] Gheitasi A, Ozbulut O E, Usmani S, et al. Experimental and analytical vibration serviceability

assessment of an in-service footbridge. Case Studies in Nondestructive Testing and Evaluation, 2016, 6: 79-88.

[29] Živanović S, Díaz I M, Pavić A. Influence of walking and standing crowds on structural dynamic properties. Proceedings of IMAC-XXVII, Orlando, 2009: 9-12.

[30] Lai E, Gentile C, Mulas M G. Experimental and numerical serviceability assessment of a steel cantilever footbridge. Journal of Constructional Steel Research, 2017, 132: 16-28.

[31] Cao L, Liu J, Li J, et al. Experimental and analytical studies on the vibration serviceability of long-span prestressed concrete floor. Earthquake Engineering and Engineering Vibration, 2018, 17(2): 417-428.,

[32] Wang,D., Wu C, Zhang Y, et al. Study on vertical vibration control of long-span steel footbridge with tuned mass dampers under pedestrian excitation. Journal of Constructional Steel Research, 2019, 154: 84-98.

[33] Chen J, Liu Q, She X. Field measurements and assessment of vibration serviceability of as-built long-span concrete floor. International Journal of Structural Engineering, 2012, 3(1-2): 61-74

[34] Murray T M, Allen D E, Ungar E E, et al. Vibrations of steel-framed structural systems due to human activity. American Institute of Steel Construction, 2016.

[35] Zhu Q K, Hui X L, Du Y F, et al. A full path assessment approach for vibration serviceability and vibration control of footbridge. Structural Engineering and Mechanics. 2019,70(6):765-779

[36] Fujino Y, Pacheco B M, Nakamura S I, et al. Synchronization of human walking observed during lateral vibration of a congested pedestrian bridge. Earthquake Engineering and Structural Dynamics, 1993, 22(9):741-758.

[37] Živanović S, Díaz I M, Pavić A. Influence of walking and standing crowds on structural dynamic properties//Proceeding of Conference & Exposition on Structural Dynamics (IMAC XXVII). 2009.

[38] Scafetta N, Marchi D, West B J. Understanding the complexity of human gait dynamics. Chaos: An Interdisciplinary Journal of Nonlinear Science, 2009, 19(2): 026108.